ENGINEERED SYNTHESIS OF NANOSTRUCTURED MATERIALS AND CATALYSTS

William R. Moser, Josef Find, Sean C. Emerson, and Ivo M. Krausz

Department of Chemical Engineering, Worcester Polytechnic Institute, Worcester, Massachusetts 01609

ADVANCES IN CHEMICAL ENGINEERING, VOL. 27 0065-2377/01 $35.00

The unusual structural and electronic properties of nanostructured materials, as they relate to recent observations of enhanced catalytic reactivities, are examined. The data suggest a need for advanced synthetic nanostructured materials processes producing high-purity crystallites in variable grain sizes in the range 1–20 nm. Within the past 5 years a wide variety of new processes have been discovered, and their capabilities are compared. One novel approach has been centered on adjusting the fluid dynamics of fast-flowing, liquid-slurry streams to conduct nanostructured materials synthesis within a cavitating bubble zone. The results of the synthesis method is to produce high shear and in situ calcination by shock wave heating and high Reynolds numbers. Nanostructured materials produced by hydrodynamic cavitation resulted in exceptionally high phase purity. In most cases, finished nanostructured metal oxides flowed directly from the processor, requiring little or no postsynthesis calcination. In many cases, the grain sizes of metal oxides and supported metals could be adjusted in the range 1–20 nm, and crystallographic strain could be systematically introduced in several classes of materials such as titania, CuO in Cu Zn Al O methanol synthesis catalysts, and piezoelectric materials. The method is inherently a high-volume, continuous process.

I. Introduction

Both the discovery of new synthesis processes for nanostructured materials and the demonstration of the highly reactive properties of these materials have increased rapidly within recent years. The new synthesis processes have made available nanostructured materials in a wide variety of compositions of metal oxides and metals supported on metal oxides, which have led to recognition of their exceptional chemical, physical, and electronic properties. The objective of this review is to provide recent results on synthesis of nanostructured materials using the novel processes that were developed in these laboratories recently and to contrast them to other important, new methods. Because some of the most important applications of nanostructured materials are as catalysts for chemical processing, several key reports on enhanced catalytic reactivity of nanostructured grains will be discussed along with the pertinent theory responsible for controlling both activity and selectivity of these new catalysts.

Over the past 30 years, our laboratory has examined the synthesis of nanostructured materials for advanced catalysts. The first process for the synthesis of fine grains of cobalt molybdates for hydrodesulfurization catalysis

(Moser, 1977, 1978a) involved a supercritical fluid synthesis of a special form of alumina having all octahedral Al^{3+} on its surface. This permitted the facile growth of Co and Mo onto this surface to provide a bimetallic structure. Using similar techniques, this type of alumina was combined with a wide variety of rare earth metal ions for HDS catalysis (Moser, 1978b,c), in which the dispersion of the rare earth oxide over the nanostructured metal oxide support was high. The next catalyst synthesis process developed was the high-temperature aerosol decomposition (HTAD) process (Moser, 1991, 1993; Moser and Cnossen, 1992; Moser and Connolly, 1996; Moser *et al.,* 1993, 1994, 1996a; Moser and Lennhoff, 1984, 1989) and was based on an early patent by Ebner (1939, 1951, 1953) used for the synthesis of simple metal oxides for ceramics applications. This process had the advantage of synthesizing nanostructured grains of simple and complex metal oxides but also resulted in high-phase purities of multimetallic perovskite, spinel, and scheelite materials. Furthermore, it resulted in metastable nonthermodynamic phases due to the fine crystallite grains in higher alcohol synthesis catalysts (Moser and Connolly, 1996) and maleic anhydride, V–P–O, catalysts (Michalakos *et al.,* 1995; Moser, 1996). High-powered ultrasound was used in the synthesis (Emerson *et al.,* 1998) of a wide variety of metal oxides and supported metal catalysts. The high-shear environment and shock wave heating provided by acoustically generated cavitation resulted in catalyst grains that were in all cases smaller than classically prepared materials, and the method resulted in Au–Pt alloys supported on titania in much higher alloy phase purity (Emerson *et al.,* 1998) compared to classical synthesis. In recent years, we discovered that hydrodynamic cavitation generated by mechanical means (Moser, 1995a,b; Moser *et al.,* 1995b, 1996b; Sunstrom *et al.,* 1996) could be used to synthesize advanced catalysts, ceramics, and electronic materials in high-phase purities and as nanostructured grains. The most recent process discovered in our labs utilized a new device for the mechanical generation of cavitation (Moser *et al.,* 1999), in which the bubble dynamics, shock wave, and shear could be controlled over an exceptionally wide range using equipment manufactured by Five Star Technologies and invented by Kozyuk (1996, 1998, 1999a–d, 2000a,b). This equipment offers the opportunity to use a range of engineering techniques and fluid dynamics phenomena to control the synthesis of nanostructured materials. This is the principal emphasis of this report and is described in Section IV.A.

II. Properties and Reactivities of Nanostructured Materials

An examination of recent information on the properties, structures, and reactivities of nanostructured materials indicates the importance of

discovering new synthetic procedures to fabricate such materials. Experimental data on the properties and catalytic reactivities of nanostructured materials reported within the past 5 to 10 years, coupled with theoretical computations in the older literature, demonstrate the significance of nanostructured materials having primary, crystallographic grain sizes in the range 1–20 nm. To put this discussion of novel synthetic techniques into perspective, a short review of the properties and reactivities of nanostructured materials will be given.

A. Structure and Electronic Properties of Nanostructured Materials

Although Baetzold's (1971, 1973) molecular orbital calculation performed nearly 30 years ago predicted that the ionization potential of nanostructured metals should increase as their grain sizes decrease, only recently has this been verified experimentally. Measurements on several metals having cluster sizes ranging from 2 to 140 atoms (de Heer, 1993) showed a systematic increase in the ionization potential for all metals studied as the cluster size decreased. The ionization potential of a 140-metal-atom cluster of Al increased from 4.7 to 6.5 eV for a 5-atom cluster. In our view this is an exceptionally important finding because it suggests that by systematically changing the grain size of a metal or supported metal through synthesis, one should be able to adjust the overlap integral between the donating metal electrons contained in nonbonding orbitals and the empty antibonding orbitals of a substrate so that an optimum energy relation exists for electron transfer and activation of either a catalytic or noncatalytic reaction. The basic theory for noncatalytic systems was described by Woodward and Hoffmann (1970), and the relationship of metallic band theory to reacting substrates was described by van Santen and Niemantsverdriet (1995). The data and reaction theory suggest that a key requirement of any nanostructured materials synthesis process is the capability to systematically vary the grain size of the crystallites between 1 and 20 nm without changing the chemistry by which the particles are produced. If this can be accomplished, the ionization potential of the different nano-sized grains can be adjusted for most catalytic reactions for optimum metal–substrate activation and maximized rates.

The high metal atom surface-to-volume ratio observed in nanostructured materials not only has importance to the number of active sites in a catalyst, but also can influence the oxygen and other anion-defect chemistry and the observation of metastable phases. Siegel's (1991, 1994) computations indicated that the percentage of metal atoms on the surface of a crystallite increased from a few percent in a 100-nm particle to about 90% in a

1-nm grain. The importance of this observation is that it predicts that surface free energy should dominate phase formation in nanometer grains of crystals rather than bulk thermodynamics. It predicts that metastable phases should be observed for many nanostructured materials. Our own aerosol synthesis (Moser and Connolly, 1996) of spinels resulted in the formation of nanostructured, metastable grains of a cubic spinel over the entire substitution series from $x = 0.0$ to 0.90, $Cu_xZn_{1-x}Cr_2O_4$, instead of the tetragonal phase. The synthesis of zirconia by hydrodynamic cavitation (Moser *et al.,* 1995b) resulted in fine crystallites of cubic zirconia that transformed to the monoclinic phase upon heating. Furthermore, the aerosol synthesis (Moser and Cnossen, 1992) of both MoO_3 and Bi_2O_3 resulted in the formation of metastable β-MoO_3 and β-Bi_2O_3 as nanostructured grains, which transformed to their respective α-structures upon calcination and grain growth. This aspect of nanostructured catalyst synthesis offers the possibility for the formation of high-temperature stable, metastable compositions for application in high-temperature turbine combustion. The high surface atom–to-volume ratio of nanocrystalline ceria was suggested (Tschöpe *et al.,* 1996) to be responsible for its high oxygen defect concentration and surface conductivity. This aspect is especially important to hydrocarbon partial oxidation catalysis because it affords the high oxygen mobility to balance the surface oxidation and reduction processes required for selective catalysis, but it also provides defect coordination sites for reacting molecules..

The change in grain size of a nanostructured catalyst results in the formation of cluster structures having stabilities that vary with grain size (Allpress and Sanders, 1970; Henry *et al.,* 1997; Montejano-Carrizales and Moran-Lopez, 1992). The consequence of this variation is that the fraction of (111) and (100) crystallographic planes varies according to the fraction of icosahedron or truncated octahedral phases of supported metals. Naturally, these crystallographic planes show very different catalytic reactivities, depending on the reaction under consideration. A more important consequence of the decrease in grain size is the observation by van Hardveld and Hartog (1972) that as the crystallite size of a material decreases, the fraction of atoms in coordinatively unsaturated edge sites relative to atoms in the stable basal planes increases to dominate the atoms exposed to a reacting gas. Indeed, in propylene selective oxidation it was shown that as the crystallite size of MoO_3 was systematically decreased, exposing more of the (100) crystallographic edges, both the activity and the selectivity for forming acrolein increased (Volta *et al.,* 1979; Volta and Tatibouet, 1985). However, for some catalytic processes, a small grain size can work to the detriment of selectivity. Okuhara and co-workers (1993) showed that exposing more of the edge sites of a V–P–O catalyst in the direct oxidation of butane to maleic anhydride resulted in a sharp decrease in selectivity.

B. Catalytic Properties of Nanostructured Materials

The preceding discussion points to a strong relationship between catalytic activity and selectivity that is controlled by grain-size effects. Although many studies, which are summarized later, have clearly demonstrated that turnover numbers (TON) greatly increase as the grain sizes decrease, the factors responsible for the observed rate acceleration have not been elucidated. The preceding discussion suggests that some of the controlling factors responsible for rate acceleration are (1) the increase in coordinatively unsaturated edge sites as grain sizes decrease, (2) the more favorable energy relationship between electrons on the metal or metal oxide surface and the antibonding orbitals of the substrate to be activated, (3) a higher concentration of anion vacancies and defect sites on the crystallite surface, (4) the higher electrical conductivity and ion mobility of nano-crystallite surfaces, (5) a higher degree of crystallographic strain as crystallites become smaller, and (6) alteration of the concentration of crystallographic planes of greatly differing activities as the catalyst crystallite size changes in the region 1–20 nm. In the following section, a few examples of a decrease in a catalyst's grain size leading to increased reactivity per metal atom center are given; however, there are some cases reporting that a decrease in the grain size resulted in a volcano plot, where reactivity decreased as the particle approached the 1- to 3-nm level. This phenomenon is expected if there is quantum mechanical control over the reactivity or when the particle becomes so small that it reacts with the support surface to generate a less reactive metal center.

The literature reports several cases where unusual catalytic properties resulted when nanostructured materials were compared to micrometer-size grains. When 1- to 5-nm particles of rhodium were synthesized on a polymer support (Busser *et al.,* 1996) and studied for their activity to hydrogenate cyclohexene, the turnover number smoothly increased by a factor of 10 as the particle size decreased from 5 to 1 nm. The synthesis of TiO_2 as nanometer grains by an aerosol process (Wold *et al.,* 1996) resulted in greatly enhanced activity as a photocatalyst for the decomposition of chlorocarbons. Thin films of TiO_2 were fabricated by spray pyrolysis techniques and were found to be especially active for chloro-organics photodecomposition. A sample of MoS_2 prepared with a high edge-to–basal plane ratio as 5- to 25-nm crystallites by an exfoliation technique led to a hydrodesulfurization activity that was four times greater than that of a large crystal of MoS_2 (Del Vallee *et al.,* 1994). Nanometer-size grains of supported iron and palladium catalysts (Wilcoxon *et al.,* 1993b) prepared by a micelle technique showed that pyrene was hydrogenated progressively faster up to two orders of magnitude in rate ratios when the particle sizes of palladium were systematically decreased from 14 to 3 nm. The preparation of gold particles in different grain sizes on titania

and iron oxide supports led to catalysts that were substantially more active (Haruta, 1997; Haruta *et al.,* 1993; Sanchez *et al.,* 1997; Tsubota *et al.,* 1994, 1995) and more stable for CO oxidation. The gold particles were found to be in a separate phase from the support and were a few nanometers in grain size. As the grain size was reduced from 8 nm to the 3-nm range, the reactivity increased dramatically. Other Au studies (Sze *et al.,* 1993) on CO oxidation on iron oxide of different morphologies showed that both grain size and the degree of roughness of the catalyst were important in controlling the CO oxidation activity. Grain sizes of 2–6 nm exhibited nearly twice the rate of 3- to 8-nm particles, and very uniform Au particles demonstrated a very low rate. In addition, the nonuniform Au particles deactivated at a much lower rate than uniform ones. Suslick and co-workers (Grinstaff *et al.,* 1992; Suslick *et al.,* 1994) reported the synthesis of nanometer grains of iron particles prepared by acoustic sonochemical means. These catalysts were prepared by sonolysis of $Fe(CO)_5$ in high surface areas as amorphous metallic particles due to the high heat-up and cooling rates inherent in the cavitation effect. They were much more effective than classically prepared materials in syngas conversion and hydrocarbon dehydrogenation.

Studies on the formation of metal clusters between 1 and 50 atoms by ion-bombardment techniques (Kaldor and Cox, 1990) led to several interesting phenomena as the number of atoms in the clusters decreased into the range 3–15 atoms. Deuterium adsorption studies showed that the H/M ratio greatly increased as the number of metal atoms per cluster decreased into the 10-atom range and greatly accelerated between 3 and 5 atoms for Rh, Pt, and Ni clusters. Similar preparations of Pt and Pd clusters were evaluated for their reactivity with methane (Cox *et al.,* 1990). Pt clusters showed a marked increase in reactivity below 8 atoms per cluster, whereas the Pd clusters exhibited a maxima between 10 and 15 atoms. Doesburg and co-workers (1987) synthesized copper supported on alumina-stabilized zinc oxide in grain sizes ranging from 3 to 20 nm. When these catalysts were evaluated for their methanol synthesis activity, a smooth increase in their turnover numbers resulted as the grain size decreased but showed a maxima at 4.5 nm. Smaller grain sizes resulted in much lower reactivities. Such a decline in activity for very small particles was observed in butane hydrogenolysis and hydrogen adsorption by nanostructured Pt supported on fine grains of titania (Salama *et al.,* 1993). The studies showed that the platinum was better dispersed as the titania grain size decreased, and the catalytic reactivity increased at lower Pt grain sizes down to 4 nm. Electron spin resonance studies showed that the reason for the reduction in activity for Pt below 4 nm was due to an SMSI surface reaction of Pt(0) with titania to form a partially oxidized Pt atom and formation of surface Ti^{3+}. Likewise, the hydrogenation of benzene by Rh supported on alumina (Fuentes and

Figueras, 1980) in grain sizes from 11 to 1 nm showed that as the Rh grains decreased from 11 to 4 nm, the TON increased, but it then sharply decreased from 4 to 1 nm. Benzene hydrogenation on Ni supported on MgO showed no such volcano plot (Nikolajenko *et al.,* 1963). Although the Ni grain sizes were not measured, the hydrogenation rate per metal atom in the samples smoothly increased by a factor of 20 as the Ni concentration was decreased from 80 to 1%. Masson *et al.* (1986) reported that ethylene hydrogenation by Pt on alumina exhibited an increase in TON by a factor of 6 as the grain size of Pt decreased from 2.5 to 0.5 nm, which decreased by a factor of 2 at slightly lower grain sizes.

Our conclusion from these properties and reactivity considerations is that the discovery of nanostructured synthesis processes that afford systematically varying grains in the range 1–20 nm is exceptionally important to the discovery of highly active and selective catalysts. It is evident from the general catalysis literature that if one is to be able to observe systematic changes in catalytic performance as a function of the degree of ion modification, one must use synthetic techniques that ensure a high degree of phase purity. This requires a high degree of mixing of ions during the synthesis step or avoidance of phase separation during this step. Naturally, the optimum situation is to achieve homogeneous solid solutions after calcination to the temperature where the catalytic process operates. Fortunately, most nanostructured synthesis processes produce materials having high phase purities, whereas most classical methods of synthesis result in rather poor phase purities.

III. Progress in Synthesis Processes of Nanostructured Materials

Due to the recent identification of the unusual reactivities and structural properties of nanostructured materials, progress the syntheses of such materials by entirely new approaches and modifications of older methods has greatly accelerated. The older methods have recently produced nanostructured grains (smallest crystallites) and particles (agglomerates of fine crystals) in controlled morphologies due to a concentration on the chemistry required for the formation of fine grain materials. Many of the newer processes have required the development of special hardware and equipment to give particle isolation through metal vaporization or molecule vaporization, metal ion dispersion and mixing through inducing a high shear environment during synthesis, atomic scale separation of the metallic components through surfactant coordination or supercritical fluid processing, or the introduction of low concentrations of mutually insoluble solid-state

phases during the synthesis step. Many of the more important methods are described in the following sections.

A. Sol–Gel and Precipitation Technologies

Continuing progress is being made in the synthesis of nanostructured materials by sol–gel techniques in the synthesis of nanolaminates (Sellinger *et al.,* 1998) and solution-precipitation techniques (Schultz and Matijevic, 1998). The advantage of the sol–gel method of synthesis is that virtually any metal oxide system can be examined, and no special apparatus or equipment is required. The advantages of sol–gel processing are the formation of ceramics of high purity and good control over microstructure and particle morphology in the synthesis, typically at room temperature. Matijevic (1992) has shown that the precipitation of colloids may be accomplished in a wide variety of morphologies and grain sizes; however, in order to obtain different morphologies and sizes, extensive chemical modifications must be made for each metal oxide system studied. The sol–gel technique works well for the synthesis of complex metal oxides with high phase purity because the polymerizing gel traps the various metal ion components spatially, permitting precipitation from solution where all the metal ions occupy near-neighbor positions in the gel matrix. Upon further processing and high-temperature calcination, the resultant amorphous mixture of metal oxides, hydroxides, and metal salts decomposes with M–O–M bond formation, while having to diffuse only a few angstroms to their lattice positions in a homogeneous solid solution. Furthermore, the gel matrix isolates the individual metal oxide particles, giving rise to nanostructured grains after the high-temperature calcination to form the finished metal oxide. Other methods use organometallic precursors having well-defined numbers of metal ions in their organometallic clusters as either mono or multimetallic complexes.

A study (Zhang *et al.,* 1998) on the synthesis of nanostructured titania reported that the introduction of low concentrations of iron during the precipitation step resulted in anatase having photocatalytic activity considerably higher than that of materials containing no Fe. Samples were prepared in grain sizes of 6, 11, and 21 nm by carrying out the hydrothermal synthesis at different temperatures and times, and the variation of Fe between 0.0 and 1.0 resulted in minor changes in grain sizes. The study further showed that despite the pure anatase crystal structure, the photonic efficiencies for the photocatalyzed decomposition of $CHCl_3$ were higher than those of standard catalysts, and there was an optimum iron concentration for maximum photocatalytic reactivity for each titania grain size. Furthermore, the photonic

efficiency for pure anatase catalysts having no Fe ion doping with grain sizes between 6 and 21 nm afforded a reactivity maxima at near 11 nm.

A careful and systematic study (Wang and Ying, 1999) on titania synthesis showed that adjusting the water/alkoxide ratio in a classical precipitation of titania resulted in pure anatase materials after calcination at 723 K for 2 h, which exhibited grain sizes varying from 82 to 14 nm as the water/alkoxide ratio was systematically increased from 3.3 to 165. A modification of the classical precipitation process by precipitation followed by hydrothermal treatment at different temperatures resulted in pure anatase, which varied in grain size from 6 to 28 nm as the hydrothermal treatment temperature was increased from 353 to 513 K. Surprisingly, the 353 K hydrothermal treatment resulted in a material that remained pure anatase phase after calcination in air at 1073 K for 2 h. The sample experienced a modest grain growth from 10 to 35 nm. Performing the hydrothermal treatment in an acidic media made it possible to convert the samples to pure rutile, although the grains grew to 49 nm.

B. Combustion Flame–Chemical Vapor Condensation Process

The CF-CVC (combustion flame–chemical vapor condensation) process developed by Kear and co-workers (Skandan *et al.,* 1996; Tompa *et al.,* 1999) is a continuous process using the equipment shown in Fig. 1. The starting materials are metal complexes that can be vaporized and fed into a flat flame, which immediately converts the compounds to nanostructured metal oxides. The particle dilution is controlled to prevent agglomeration in a hot state

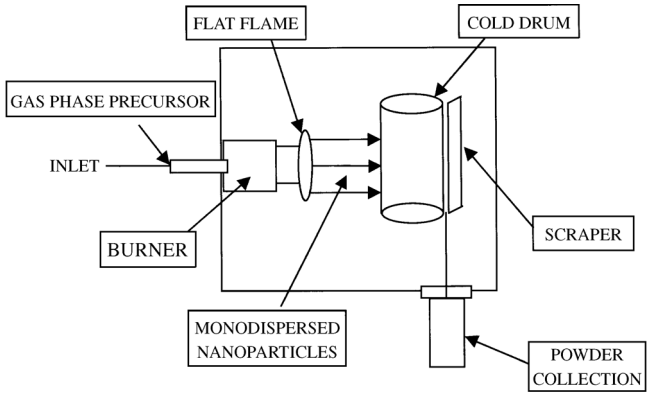

Fig. 1. The CF-CVC (combustion flame chemical vapor condensation) (Skandan *et al.,* 1996; Tompa *et al.,* 1999) for producing nanostructured materials.

in the flowing gas stream. The solid particles are then collected on a cold surface and scraped off continuously into a powder bin. A variety of simple and complex metal oxides have been produced in this way, including silica, alumina, titania, barium titanate, zinc, and copper oxides. This process is similar to the earlier-reported Cabot process (Jordan *et al.,* 1990), but it uses advanced flame design and control to afford better dispersion of the nanostructured grains. Particle sizes were generally in the 20-nm size range, although they could be controlled between 3 and 75 nm for some systems through variation of temperature, precursor flow rates, and pressure in the chamber.

The Cabot flame process (Jordan *et al.,* 1990) for the production of high-surface-area nanostructured materials is mentioned here because the technology is of great potential importance to the general synthesis of nanostructured materials. Although the technology is not current and has apparently been abandoned by the developers, we regard the approach as being exceptionally important and not generally recognized in the literature. The process atomizes a solution of a decomposable metal salt or metal salt mixture by mixing with a high-Mach-number gas at high temperature. The gas is created by high-temperature combustion of an appropriate fuel using technology developed by Cabot in other processes. The data reported for alumina synthesis indicated that high Mach numbers led to 165 m^2/g foamed alumina. The surface area of the alumina could be systematically varied between 17 to 165 m^2/g by altering the gas velocity and combustor temperature. The report also described the flame synthesis of titania and zirconia.

C. Gas Phase Condensation Synthesis

The newest development in the gas phase condensation process involved the use of dc- and rf-magnetron sputtering (Tschöpe *et al.,* 1997; Ying and Tschöpe, 1996) to introduce metals into the gas phase instead of induction heating used by Gleiter (Birringer *et al.,* 1984; Gleiter 1981, 1989) and Siegel (1991, 1994; Siegel and Hahn, 1987). The equipment used in this type of process is similar to that shown in Fig. 1 except that the starting material is usually a pure metal that is introduced into the vapor phase by various heating methods. The metal vapor is then transported by an assisted gas stream onto a cold surface where it is collected. The resultant powder may be used as is or subjected to a controlled oxidation to produce the nanostructured metal oxides. An unusually high degree of oxygen nonstoichiometry was observed in the vapor-phase synthesis (Tschöpe *et al.,* 1996, 1997; Ying and Tschöpe, 1996) of CeO_{2-x} compared to conventional precipitation synthesis. Also the grain sizes were smaller (8 nm vs 8–12 nm), and surface areas were

larger than those of conventional materials. The catalytic properties of the cerium oxide nanocrystals were investigated for SO_2 reduction, where a considerable reduction in light-off temperature was observed (Tschöpe *et al.,* 1997).

Berthet *et al.* (2000) examined the deposition of palladium on a silicon carbide support (SiC) using both a high-frequency (100-MHz) plasma-sputtering technique and a metal atom beam deposition in which the Pd was evaporated onto the SiC surface. The former technique resulted in the deposition of 2.5-nm spherical crystallites on the surface, whereas the Pd atom vaporization resulted in the formation of thin stacked monolayers on the surface. In both cases, based on X-ray photoelectron spectroscopy, the low-level metal-deposited samples showed an interaction of Pd with the SiC surface. Butadiene hydrogenation using these catalysts showed that as the metal concentration on the surface increased, the turnover frequencies (TOF) increased. The synthesis studies were carried out to generate a nanostructured catalyst particle that is in close proximity to a SiC surface, an excellent heat-transporting material. The idea was to determine whether the fine-grain Pd–SiC would be beneficial in removing local heat generated in strongly exothermic hydrogenation reaction. The catalytic reactivity data showed that the thin monolayer structure (atom vapor) rather than the larger three-dimensional crystallites (plasma) resulted in far more active catalysts.

D. Reverse Micelle Synthesis

The reverse micelle approach continues to grow in importance in the synthesis of nanostructured materials. The basis for the technique is the use of a surfactant to stabilize varying aqueous droplet sizes in a hydrocarbon medium. Metal salt precursors are contained in the aqueous portion and are transformed by a reactant from the hydrocarbon phase. Both the structure of the surfactant and the steric size are able to produce metals having a wide range of grain sizes. Although notable grain-size control has been observed, the technique has a major disadvantage in that the commercial application may be limited due to the large amount of organic surfactant surrounding the crystals, and when this is removed by washing, the nanostructured metal grains normally grow.

Poly(oxyethylene)nonylphenyl ether (Igepal-20) has been used in a combined synthesis of nanometer grains of silver on fine-grain silica (Li *et al.,* 1999b). This method uses Igepal in a hexane solution with silver nitrate dissolved in the aqueous phase. Hydrazine hydrate is then added to reduce the Ag after the fine droplets of micelle have been formed, resulting in metallic silver particles contained inside the micelle. Then tetraethylorthosilicate

(TEOS) is added in cyclohexane: it is slowly hydrolyzed by the water inside the micelle, resulting in nanometer-sized grains of Ag supported on monodispersed spherical grains of silica. The advantage of the technique is that the grain size of the Ag can be systematically changed from 12 to 125 nm by altering the water/Igepal or water/TEOS ratio.

Martino and co-workers at Sandia National Lab have developed a new wrinkle in their previously reported (Martino *et al.,* 1995, 1997; Wilcoxon *et al.,* 1993a) inverse micelle synthesis of nanostructured reduced metals. Those studies showed that nanometer-size grains of supported iron and palladium catalysts could be prepared in varying grain sizes by a normal inverse micelle technique and that nanostructured palladium hydrogenated pyrene progressively faster, up to two orders of magnitude in rate ratios, when the grain sizes were systematically decreased from 14 to 3 nm (Wilcoxon *et al.,* 1993a). The new synthetic method (Martino *et al.,* 1999; Sault *et al.,* 2000) combines the inverse micelle technique with a standard sol–gel synthesis. For the synthesis of nanostructured grains of Pt/silica, an inverse micelle is formed using a surfactant in hexane–water. Then $PtCl_2$ and TEOS are mixed in, and the resultant reverse micelle is reacted with $LiBH_4$ in tetrahydrofuran (THF) to reduce the metal ion. This mixture is gelled using tetrabutylammonium hydroxide (TBAOH) and further processed by sol–gel techniques. Both Pt/silica and Pt/alumina were synthesized in grain sizes around 2 nm before calcination and 3.5–4.5 after a 723 K air calcination. Another report suggests that the technique can be used for other reduced nanostructured metals (Martino *et al.,* 1998).

A detailed study (Zarur *et al.,* 2000) of the reaction variables of a reverse microemulsion synthesis of barium hexaaluminate (BHA) resulted in nanostructured grains that could be varied over the range of 5 to 120 nm after calcination to 723 K and surface areas that ranged from 20 to 100 m^2/g after air calcination to 1573 K. The variability was obtained by altering the water concentration in a synthesis using a nonionic surfactant of polyethoxylated alcohols and barium and aluminum alkoxides as precursors. A narrower range of grain sizes of 4 to 12 nm was realized by altering the water-to-alkoxide ratio, and this variability led to surface areas after the 773 K calcination of up to 600 m^2/g. Furthermore, ceria in concentrations up to 25% w/w could be deposited on the aluminate without significant agglomeration after 1573 K calcination (Zarur and Ying, 2000). The ceria grains after calcination at 1073 and 1573 K were 6 and 20 nm, respectively. An examination of the methane total catalytic combustion activity of these catalysts showed (Zarur and Ying, 2000) that the BHA prepared by the reverse micelle technique resulted in a 110 K lower light-off temperature than a classically prepared sol–gel synthesis, and the ceria-modified reverse micelle BHA afforded a catalyst with a light-off temperature about 300 K lower.

E. Polymer-Mediated Synthesis

A potentially important, new nanostructured metal-particle synthesis technique based on mediation by polymeric materials might overcome the problems associated with the large amounts of surfactants required in micelle processes. The general synthetic technique is based on the reduction of a platinum salt (Zhao and Crooks, 1999a) or palladium salt (Zhao and Crooks, 1999b) with aqueous $NaBH_4$ in the presence of a hydroxyl-terminated dendrimer. Dendrimers are monodispersed, hyperbranched polymers having a very high concentration of surface functional groups. Twelve to 60 Pt^{2+} atoms can be loaded into a poly(amidoamine) dendrimer (PAMAM) and reduced to the metallic nanostructured grains. The interesting aspect about this method of synthesis is that the reduced metal could be extracted in to hydrocarbon solution, leaving the polymer behind. Nanostructured metals prepared by this technique have been found effective as catalysts for electrolytic O_2 reduction and allyl alcohol hydrogenation. In a review of the most recent findings Crooks and co-workers (2000) described a wide range of reduced metal-loaded particles in varying particle sizes for dendrimers containing Cu, Pt, Pd, Ru, Ni, and Ag. Depending on the degree of growth in the polymerization process, reduced metals of different cluster sizes could be formed in dendrimer formation. Furthermore, different cluster sizes could be produced by altering the amount of metal originally used in forming the dendrimer–metal complex. For example, the synthesis of Pt/dendrimers containing 40 and 60 Pt atoms within the internal structure of the dendrimer resulted in particle diameters of 1.4 and 1.6 nm, respectively. Characterization of these particles as well as Pd/dendrimers showed that the particles were monodispersed and spherical. Reduced silver particles could not be prepared directly but were obtained through *in situ* reduction of Ag^+ in solution by a reduced Cu(0)/dendrimer. Either displacement methods or direct synthesis techniques were successful in synthesizing bimetallic reduced-metal particles within dendrimers containing Au/Cu, Pd/Cu, Pt/Cu, and Pt/Pd nanoparticles. Catalytic studies for heterogeneous oxygen catalyzed reduction by 60 Pt-atom-dendrimer nanoparticles resulted in facile O_2 reduction. Due to the differing steric properties in dendrimers under different polymerization conditions, different rates of hydrogenation and selectivities between linear and branched olefins were observed. The 40-atom Pd/dendrimer catalysts resulted in turnover rates similar to those of polymer-bound Rh^+ catalysts, and when the 40-atom Pd catalyst was used after preparation from dendrimers of higher degrees of polymerization, a selectivity of the linear to branched olefins was observed. The previously mentioned catalytic studies were carried out in aqueous solutions; however,

several techniques were developed to generate catalysts that were stable and catalytically active in organic media. Upon functionalization by perfluorinated polyethers, Pd nanoparticles within dendrimers could be solubilized in supercritical CO_2. Catalytic studies under supercritical conditions resulted in a much more selective catalyst for the Heck coupling of arylhalides and methacrylates, as compared to the homogeneous Pd-catalyzed reaction. One potential problem with this type of nanostructured catalyst synthesis is the fact that the polyamidoamine dendrimers have a maximum thermal stability of only 373 K, whereas the polypropyleneimine dendrimers are stable to 743 K.

Another polymer-mediated synthesis used a lyotropic liquid-crystal (LLC) template to obtain 4- to 7-nm crystallites of Pd (Ding and Gin, 2000). In this study, Pd^{2+} was ion exchanged into the channels of a cross-linked LLC and reduced with H_2. The resultant catalysts were found to be active for efficient hydrogenation of benzaldehyde.

F. Protein Microtube–Mediated Synthesis

Behrens and co-workers (1999, 2000) are developing a new process for the synthesis of nanostructured metals and alloys in varying grain sizes supported on hollow, highly oriented protein templates. The technique uses the protein α,β-tubulin after a self-assembly into 25-nm-diameter microtubes that are several micrometers long. The surface of the protein contains thiol and ammonium end groups, which are reacted in aqueous solution with Na_2PdCl_4, followed by citrate reduction. A schematic of the process is given in Fig. 2. The grain size of the palladium synthesized in this way was reported

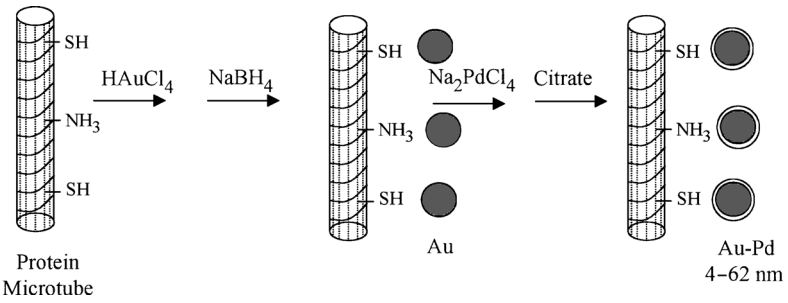

FIG. 2. Schematic of the synthesis of nanostructured metals and alloys in varying grain sizes supported on hollow, highly oriented protein templates (Behrens, Dinjus, and Unger, 1999; Behrens *et al.,* 2000).

to be 2 nm. A similar synthesis resulted in 2-nm Au particles. Upon treatment of the microtubes with $HAuCl_4$, followed by $NaBH_4$ reduction, further reaction with Na_2PdCl_4 followed by citrate reduction led to nanostructured Au/Pd alloys. By increasing the Pd/Au ratio from 2.3 to 10, the grain size of the alloy could be systematically reduced from 62 to 4 nm. The application of the alloys in crotonic acid hydrogenation in an aqueous suspension resulted in a systematic increase in the reactivity as the grain size decreased from 62 to 4 nm. The TEM data on the Au, Pd, and Au/Pd alloy particles, supported on the microtubes, appear as nanostructured grains attached to the fibrous tubes of several microns in length. Because the proteins are not stable at high temperatures, techniques were developed to support the preformed metal microtubes on alumina, which resulted in greater stability.

G. Sonochemical Synthesis

Suslick's group has made many contributions to the application of sonochemistry to the synthesis of metallic and bimetallic catalysts, which they have reviewed (Suslick *et al.,* 1999b). Other studies have turned to the synthesis of carbides, sulfides, and nitrides using the same basic technique. This method of synthesis most effectively uses as starting materials metal carbonyls, which have a finite vapor pressure. Vapor pressure of the metal component inside a bubble formed by acoustic cavitation is key to the transfer of the very high heat generated during the bubble formation and collapse. This *in situ* heat treatment converts the metal carbonyl vapors to nanostructured materials, which are especially active and selective as catalysts (Suslick *et al.,* 1996). The most recent advances have been in the sonication of metal carbonyls in the presence of reactive substrates, such as the formation of nanostructured MoS_2 by sonicating $Mo(CO)_6$ in the presence of elemental sulfur (Mdleleni *et al.,* 1998). Compared to the materials prepared by conventional synthesis, the stoichiometric MoS_2 prepared in this way demonstrated a much higher concentration of edge and defect crystallographic sites. The TEM analysis showed that the sonication-prepared MoS_2 consisted of porous aggregates of clusters of spherical particles 15 nm in diameter, whereas the conventional MoS_2 were large crystallites of well-formed layers. The catalytic evaluation of these materials for the hydrodesulfurization of thiophene demonstrated turnover numbers that were 3 to 5 times greater than those of the conventional catalyst over the range of temperatures studied from 325 to 375°C. Molybdenum carbide, Mo_2C, could be prepared as nanometer grains in surface areas of 163 m^2/g by the sonication of $Mo(CO)_6$ in hexadecane. This catalyst was examined for the hydrodenitrogenation of indole and compared to classically prepared Mo_2C

catalysts as well as Mo_2N (Li *et al.,* 1999a), and the sonication-prepared Mo_2C was slightly more active at low temperatures and less active than the conventional catalysts at high temperatures.

The sonochemical synthesis of Mo_2C was also carried out (Dhas and Gedanken, 1997b) starting with $Mo(CO)_6$ in decane in an inert atmosphere in the presence of activated silica. The resulting Mo_2C crystallites were 5 to 10 nm and coated the silica nonuniformly. A more surprising result (Dhas and Gedanken, 1997a) is the synthesis of unsupported $Mo_2O_5 \cdot 2H_2O$ (Mo^{5+}) when $Mo(CO)_6$ was sonicated in decalin under an air atmosphere. When the same reaction was carried out in the presence of activated silica (Dhas and Gedanken, 1997a, 1997b), spongy platelet nanoparticles were formed in approximately 20-nm grain sizes. The coverage by the Mo^{5+} species was uniform over the surface and tightly bound by Mo–O–Si bonds. Two other interesting results from Gedanken and co-workers (Dhas *et al.,* 1997b) was the observation that nanostructured Cr_2O_3 and Mn_2O_3 could be obtained by the sonochemical-induced reduction of the dichromate and permanganate ions in aqueous media at ambient temperatures. The materials were shown to be amorphous after the sonication; however, calcination of the Cr oxide at 900 K and manganese oxide to 600 K resulted in fine grains of the reduced oxides. The ultrasound-induced synthesis of a novel Pd/C nanostructured composition (Dhas *et al.,* 1997a) resulted when an organometallic Pd precursor was irradiated in argon in mesitylene. The structure of the composition was shown to be a carbon-encapsulated Pd core. The Pd core was 4 to 7 nm, and it was suggested that the high stability of the particles was due to the carbon overlayer.

An extensive study (Emerson *et al.,* 1998) was carried out in our laboratories on the use of high-powered ultrasound to produce nanostructured grains of metal oxides and supported metal oxides. This study examined the effects of different levels of sonication power levels, frequencies, and sonicator reactor designs to determine whether catalysts could be synthesized in controlled grain sizes. All the syntheses included the precipitation step within the high-intensity zone of an ultrasound horn, where the cavitating bubble dynamics are most concentrated. Syntheses of a wide range of nanostructured materials, such as titania, ceria, chromia, nickel oxide, cobalt oxide, alumina, zirconia, bismuth molybdates, iron oxide, and Pt/zirconia, Pt/titania, and Pt/Au alloys on titania, were performed. In all cases, the acoustic cavitational results were compared with results from classical synthesis. The comparison showed that the metal oxide grain sizes could be reduced by 2–3 nm and that, by further calcination of these materials to different levels, catalysts of systematically changing grain sizes in the region 1–20 nm could be achieved. Furthermore, by combining the cavitation experiment with some modification in the chemistry of the precipitation,

variable metal oxide grain sizes could be also realized. The study showed that the synthesis of an alloy Pt/Au catalyst over a wide range of metal compositions supported on titania could be realized as pure alloys. A direct comparison to the same range of alloy compositions resulting from the same precipitation without ultrasound power produced a significantly lower degree of alloy formation.

IV. Engineered Synthesis of Nanostructured Catalysts

Recent studies as well as research over the past 20 years in our laboratories have concentrated on the application of chemical engineering reactor design and fluid-flow technology to the synthesis of nanostructured materials as advanced catalysts. The objectives in all these synthetic studies have been to (1) obtain polycrystalline pure-phase materials, (2) synthesize the catalyst primary grains as nanostructured materials, (3) systematically vary the grain size over the range of 1 to 40 nm, and (4) discover and develop methods that are general ones not requiring an exhaustive investigation of the chemistry for each catalyst system desired to be synthesized. For all advanced catalyst work where one is attempting to improve selectivity and reactivity via metal ion modifications of a host metal oxide or alloy, phase purity is the most essential property of the synthesized catalyst. Contamination of the ion-modified catalyst by even small amounts of separate phase materials can lead to overreactivity to undesired products or deactivation of the catalyst. The importance of the nanostructured grain size, as mentioned before, is that many catalytic reactions were reported to show greatly accelerated reaction rates for samples where the catalyst primary grain sizes were in the range 1–10 nm. The importance of a catalyst preparative technique that enables one to systematically change the grain size to any value in the range 1–20 nm is that some reactions show a maximum in reactivity in this size range, and the optimum grain size differs depending on the catalytic reaction.

The classical approach to the synthesis of nanostructured catalysts and materials of different morphologies and grain sizes has been one that heavily relies on detailed experimentation, altering the chemistry of synthesis to achieve the desired material. Our view has been that this approach, although successful for the synthesis of a wide range of nanostructured materials, requires too many experiments and is generally not *a priori* predictable. As a consequence, the direction of nanostructured materials synthesis in our laboratories has been to examine the application of various mechanical techniques that have sufficient process-parameter variability to afford

systematic changes in morphology and crystallite size. Inherent in all the processes selected for study was the requirement that the method afford high-phase purity of the synthesized polycrystalline samples of nanostructured catalysts. In all the studies reported here, substantial experimentation was devoted to reactor design for each of the selected techniques to ensure that the fluid flow was well regulated so that the conversion to solid catalysts was accomplished under design conditions.

Aerosol catalyst studies (Michalakos *et al.,* 1995; Moser, 1991; Moser and Cnossen, 1992; Moser and Connolly, 1996; Moser *et al.,* 1993, 1994, 1995a, 1996a; Moser and Lennhoff, 1984, 1989) that we have conducted for more than 20 years concentrated on the development of a well-controlled continuous flow reactor, which had capabilities of regulating the contact time between 0.1 and 8 s, the capability of controlling the temperature profile throughout the reactor, and capabilities for fast quenching of products and for introduction of solid-support materials. After many prototypes were tested, an up-flow reactor design (Moser and Cnossen, 1992; Moser and Connolly, 1996; Moser *et al.,* 1994, 1995a; Moser and Lennhoff, 1989) was finalized. More than 3000 catalysts were synthesized and characterized, and the catalytic properties for many were investigated. In all cases studied, nanometer grains of materials could be synthesized by controlling the fluid-flow conditions through the reactor. The reactor was especially effective for the formation of metastable catalyst structures due to the rapid cooling capabilities. A wide range of catalysts whose compositions included 3 or 4 metal ions demonstrated that materials of exceptionally high-phase purities could be synthesized. The advantage of this aerosol process is that the feed streams used solution of the desired metal salts.

The engineering aspects of our studies on the use of acoustic cavitation to generate nanostructured catalysts centered on the design of a reactor (Emerson *et al.,* 1998) that resulted in the most effective contact of cavitating bubbles with the *in situ* synthesized catalyst gel particle. The equipment permitted control over the bubble dynamics through regulating both the ultrasound's power and frequency. The equipment design also included mixing facilities, which resulted in the synthesis of multimetallic compositions having a high degree of phase purity after calcination.

Our design of a microwave reactor for examining nanostructured catalyst synthesis involved delivering the metal salt solution to the highest energy region of the microwave radiation, where it immediately interacted with a precipitating agent. No cavitation effects are expected using this method; however, the interaction of microwave radiation on a slurry of gel particles might give rise to *in situ* particle heat-up effects, which could afford *in situ* calcination and limiting grain growth. In most cases studied, synthesis under the influence of microwave power resulted in reduced grain sizes after

calcination, as contrasted to parallel classical synthesis. For example, in the synthesis of $Bi_2Mo_3O_{12}$, $Bi_2Mo_2O_9$, and Bi_2MoO_6, a comparison of the grain sizes for the microwave to classical synthesis after 598 K calcination revealed grain sizes (microwave/classical) of 15/22, 23/37, and 36/49, respectively. A microwave synthesis of CuO and calcined at 573 K resulted in 13 nm and classical 19 nm; Co_2O_3 synthesis resulted in 13 nm microwave vs 17 nm classical after 573 K calcination. Several other syntheses were carried out; however, the inability to achieve significant reduction in grain sizes does not suggest that this method is useful for variable-grain, nanostructured synthesis at the low power levels of commercial microwave ovens.

A. Hydrodynamic Cavitation

The objective of the research on hydrodynamic cavitation was to use the high Reynolds numbers and controllable throat cavitation numbers to regulate synthesis of both metal oxides and supported metals and metal oxides. From this discussion, it is clear that for catalytic applications, it is important to control phase purity to synthesize homogeneous solid solutions, primary grain (crystallite) size, systematically variable within the range 1–20 nm, and particle (agglomerate) size control and to adjust other properties such as crystallographic strain. In general, it is desirable to obtain the highest degree of mixing of all metal-containing components during a synthesis. This is also important for dual-phase, bifunctional catalysts. Our experimental results and fluid dynamic modeling studies clearly show that controllable synthesis is observed only when the equipment used has the capability of varying the bubble dynamics over a wide range. The technique essentially does catalyst synthesis within the high-shear and high-temperature zone of cavitating bubbles generated by passing a fluid containing the precipitated catalyst precursors through a set of orifices at high velocities and high head pressures. Our general synthetic strategy is illustrated in Fig. 3; this approach applies not only to our studies on hydrodynamic cavitation but also to our studies on acoustic cavitation mediated synthesis.

The schematic in Fig. 3 shows that the synthesis starts with one solution or more containing the metal salts, such as nitrates, acetates, alkoxides, and chlorides. If the solutions are not compatible, the metal ions must be fed using multiple-feed streams. This stream is metered into a second stream containing a precipitating agent such as sodium hydroxide, ammonium hydroxide, or ammonium or sodium carbonate. Care is taken to ensure that the individual metal salts totally and immediately precipitate upon contacting

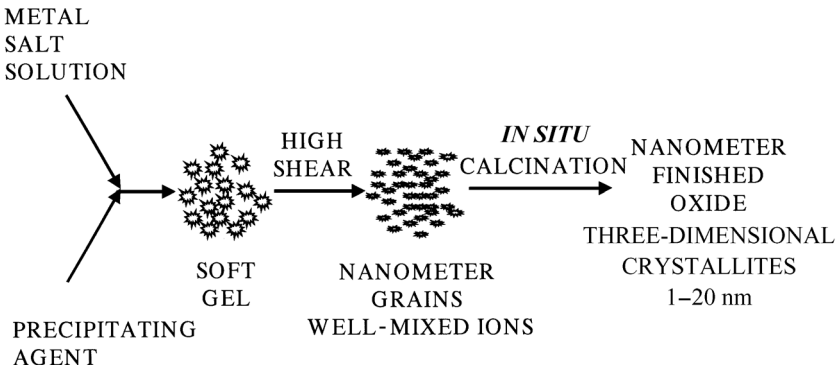

FIG. 3. Schematic of a typical hydrodynamic cavitation synthesis of metal oxides starting with a metal salt solution, which is precipitated and processed in a cavitating stream of bubbles.

the precipitating agent. This results in the formation of a soft gel contained as a slurry within a fast-flowing stream of the precipitating agent. This gel is immediately drawn into the high-pressure zone of the cavitation equipment, where the hydrostatic pressure is regulated between 0.1 and 178 MPa. The stream then passes through an orifice at near-supersonic velocities, which results in the formation of cavitating bubbles. It is the multiple collapse–reformation–collapse of these bubbles in the vicinity of the suspended soft gel that causes the high shear environment and local shock wave heating. This results in both efficient mixing of the individual metal ions and *in situ* calcination to decompose the metal salts to the oxide or hydroxide. The high shear environment also leads to a fragmentation of nanostructured grains of the materials that are agglomerated into larger clusters. The result of this method of synthesis is the formation of nanostructured grains of materials that are normally homogeneous solid solutions in the form of their oxides unless the hydroxides are more stable in aqueous media. Control of the bubble dynamics in the cavitation zone is key to the control of the grain size of the catalysts as well as their agglomerate size.

The equipment that we are currently using for hydrodynamic synthesis was invented by Kozyuk (1996, 1998, 1999a–d, 2000a,b) and manufactured by Five Star Technologies, Cleveland, Ohio. The advantage of this equipment is that it incorporates the process variability necessary to regulate the bubble dynamics required for the synthesis objective. It does this by enabling synthesis to be conducted at very high Reynolds numbers and at variable pressures that are required for adjusting the throat cavitation number and recovery pressure as well as bubble size and shock wave energies in the cavitation zone. This is done by a simple change of the combination of

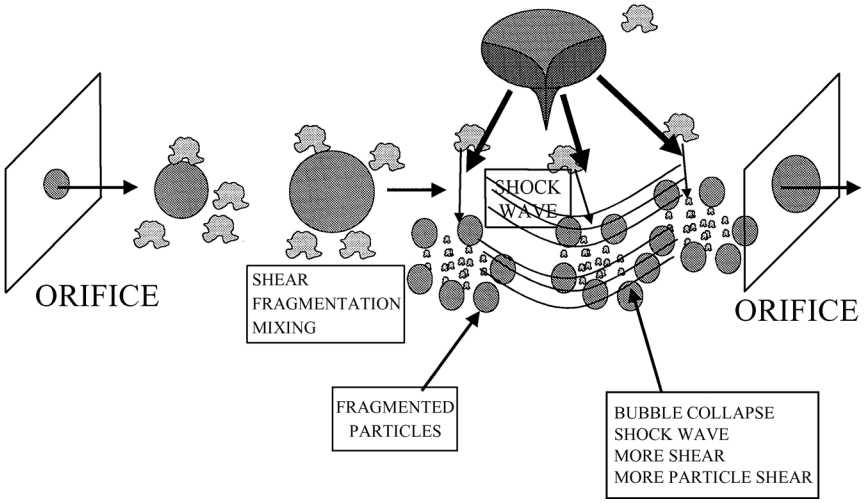

FIG. 4. Schematic of cavitation bubbles interacting with a slurry of precipitated gel particles. The configuration shows typical two orifice processing as afforded in the CaviPro 300 processor. Cavitating bubbles initially form, expand in the recovery zone, and collapse with the formation of a microjet and shock wave.

orifice sizes and geometries located on both the upstream and the downstream side of the cavitation zone. The fluid dynamics problems associated with this method of synthesis are illustrated in Fig. 4. The figure shows the gel slurry entering the first orifice on the left side of the figure. This orifice size, as well as the second orifice on the far right side of the figure, is regulated from 0.050 to 0.50 mm. The hydrostatic pressure of the slurry stream is regulated between 0.1 and 178 MPa, and the fluid flow and Reynolds number are controlled by setting the head pressure and the orifice size utilized in the experiment. When a fast-flowing slurry stream passes through the first orifice, a cavitational bubble is formed due to the Bernoulli effect. Because the second orifice size is usually larger than the first orifice, the pressure in the recovery zone or cavitational zone is less than the head pressure. This pressure difference causes the bubble initially to begin to expand. According to fast photographs taken of bubbles at much lower pressures, the bubbles then begin to turn inward, forming a pointed microjet, and implode with the formation of many smaller bubbles. These bubbles then shrink and rebound; during the rebound process they emit a shock wave (Young, 1989), which gives rise to local heating to within a few bubble radii. These bubbles then implode, and the process is repeated for many cycles. Shear is caused by the bubble formation–collapse–reformation dynamics, and the *in situ* calcination of the solids in the slurry is caused by the shock wave. Because the

metal components are not contained within the bubble-gas phase, little calcination occurs due to the high temperature generated within the bubble. The temperature within the bubble resulting from acoustic cavitation has been reported to be within the range of 2000 to 5000 K (McNamara *et al.,* 1999; Suslick, 1993; Suslick *et al.,* 1999a), which is quite effective for decomposing volatile metal carbonyls that have some vapor pressure within the bubble (Hyeon *et al.,* 1996).

The relationship of the double-orifice cavitation generator to the model shown in Fig. 4 is that alteration in the head pressure, fluid flow, and orifice sizes control the bubble dynamics within the recovery zone. Our conceptual model suggests that the bubbles need to be larger than the gel particles, the bubbles need to be under the highest pressure possible, and they must form and collapse as rapidly as possible. These circumstances are optimum for the generation of shear and shock wave calcination of the gel solids. The computational challenge is to calculate the dynamics of the bubble in a flowing system at high pressure where the initial bubble size cannot be estimated. Our fluid dynamic computations on this type of two-orifice system based on relative bubble-size changes show that our device results in the correct bubble-size regime of about a micrometer. However, the results suggest contravening effects. As the pressure within the recovery zone (regime between the first and second orifice) increases, the intensity of the pressure within the bubble increases, and the intensity of the shock wave increases. This gives more intense *in situ* gel particle heating. However, as the pressure in the zone increases, the bubble size decreases. Unfortunately, the fluid dynamic computations on this type of system are too complex currently to enable precise computations to optimize bubble energetics and dynamics. However, based on the relative bubble size computation, we conclude that synthesis studies, where properties such as grain size, agglomerate size, internal strain and phase purity are varied as a function of the orifice parameter set utilized or head pressure applied, will likely show maxima or minima in plots of the experimental results such as grain size vs head pressure. However, at this point the important aspect of the two-orifice system is the capability of the equipment to experimentally vary the dynamics of bubble collapse, and the synthesis studies reported in the next section indicate the important flow regimes.

B. Experimental

Two cavitational devices manufactured by Five Star Technologies were used for synthesis and were the models CaviMax (a single-orifice processor, operating at a constant flow rate and variable pressures) and the CaviPro 300

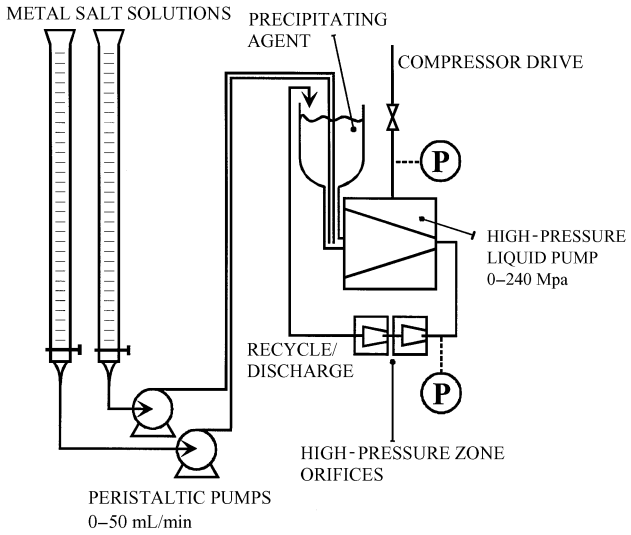

FIG. 5. Diagram of a typical flow configuration for synthesis in the CaviPro 300 processor equipped with a double-orifice cavitation chamber. Metal salt solutions are metered into a precipitating agent just before the inlet to the high pressure pump. The pressure of the solution is then raised to between 1 and 200 MPa and passed through a set of two orifices that generate cavitating bubbles. The effluent is shown to recycle back to the reservoir containing the precipitating agent.

(a double-orifice processor, having variable-pressure-adjustment capabilities). A schematic drawing of the experimental setup is given in Fig. 5.

At the start of a typical experiment, the processor was turned on to begin recirculation of a precipitating agent, which consisted of water or isopropanol containing a dissolved basic salt. Once the precipitating agent was flowing through the system, one or more metal salt solutions were metered into the cavitation device using precision peristaltic pumps, resulting in the immediate formation of a precipitated gel of the metal oxide components. The gel slurry flowed into the processor at the inlet to the high-pressure section and was recirculated during the addition of the feed streams, followed by an additional recirculation period, usually of 10 min. The temperature of the recirculating material was regulated by cooling the gel slurry with an ice bath, in the case of the CaviMax, or through the use of an in-line heat exchanger, in the case of the CaviPro 300. At the end of a synthesis, the product slurry was collected and pressure-filtered under 0.67 MPa of nitrogen on 142-mm-diameter, 0.2-μm nylon filter paper. After the initial pressure filtration, the filter cake was washed and refiltered. The washed solid was then dried overnight (at least 12 h) at 373 K. The dried materials were typically

calcined to higher temperatures in air to verify the identity of the product and to make particle size and strain estimates via X-ray diffraction.

X-ray diffraction experiments (XRD) were done with a Rigaku Geigerflex diffractometer (Bragg–Brentano geometry, reflection mode; graphite-secondary monochromator, Cu$K\alpha$ radiation, $\lambda = 154.16$ pm). The program Powder Cell was used to deconvolute phase mixtures and to simulate X-ray patterns. An Amray AMR 1610 scanning electron microscope (SEM), operating at an acceleration potential of 15 kV and an emission current of 65 μA, was used.

The family of $La_{0.6}Sr_{0.4}FeO_3$ perovskites was synthesized using the indicated stoichiometric quantities of the corresponding metal nitrate salts dissolved in water and precipitated with an aqueous solution of Na_2CO_3. A classical precipitation was done in a similar manner using a flask equipped with a mechanical stirrer.

The titania syntheses were carried out using a 0.5 mol/liter titanium tetrabutoxide solution in isopropanol, which was fed into 250 ml of water. After filtration, the samples were dried and calcined at 673 K for 4 h. The PZT samples were prepared using the indicated stoichiometric amounts of titanium tetrabutoxide and zirconium tetrabutoxide in isopropanol, which were cofed with an aqueous lead acetate solution and precipitated using an aqueous $(NH_4)_2CO_3$ solution directly in the inlet of the high-pressure pump. The addition of the solutions was completed after 20 min. The reaction mixture was then processed for an additional 10 min, giving an overall reaction time of 30 min.

C. Characterization of Reynolds and Throat Cavitation Numbers

In order to apply fluid dynamics to understand its effect on synthesis and to use this information to control the synthesis to specific chemical and morphological properties, an extensive study was undertaken to characterize the entire range of Reynolds numbers and throat cavitation numbers affordable by both of the synthesis processors. This investigation used the CaviPro 300 and the CaviMax processors manufactured by Five Star Technologies. The CaviPro 300 is a dual-orifice processor with an operating hydrostatic pressure between 1 and 200 MPa and orifices that can be readily interchanged over the range of 0.050 to 0.50 mm. Naturally, the maximum flow rate of fluid through the instrument and maximum pressure attainable depend on the size of the orifices used in the synthesis experiments. However, the bubble dynamics can be further controlled by establishing the maximum pressure for a given set of orifices and mechanically adjusting the pressure to any lower value. The

CaviMax is a constant, high-flow-rate, single-orifice instrument with a maximum pressure of 8 MPa and orifices that can be interchanged in the range of 1.25 to 2.90 mm. The bubble dynamics can be further controlled through the use of a flow-throttling valve located just after the cavitation recovery zone. Other high-volume processors are available but were not used in this study.

To characterize the fluid flow in the CaviPro 300, a constant second-orifice size of 0.356 mm was used while the first orifice was varied from 0.127 to 0.305 mm. For a given orifice set, the Reynolds and throat cavitation numbers were computed by measuring the flow resulting from adjusting the pressures just before the first orifice from a minimum value to the maximum pressure resulting from that particular orifice set. A wide variety of first orifices were studied, and to illustrate the range, the orifice set 0.127 (first) and 0.356 (second) resulted in Reynolds numbers ranging from 15,000 to 55,000 and throat cavitation numbers ranging from 1.6 to 5.6. Use of the larger first orifice of 0.305 and 0.356 in the downstream (second) position resulted in Reynolds numbers of 22,000 to 55,000 and cavitation numbers of 2.5 to 5.5. For each orifice set, both the Reynolds number and cavitation numbers were precisely adjusted over the indicated range by a simple adjustment of pressure.

Cavitation occurs when bubbles containing either vapor or gas are formed by reduction in the local pressure at constant temperature (Brennan, 1995; Knapp *et al.,* 1979; Young, 1989) such as the rapid movement of the fluid past an impeller blade, through a pump, or in this case through a restriction (orifice) at near supersonic velocities. Quantifying the cavitation number is debatable, but it can be derived from the Bernoulli equation. Lush (Young, 1989) uses a throat cavitation number (σ_{T}) defined as

$$\sigma_T = \frac{p - p_V}{\frac{1}{2}\rho u^2},$$

where p is the total upstream pressure, μ is the liquid velocity in the throat, p_{V} is the vapor pressure of the liquid, and ρ is the liquid density.

Although the onset of continuous cavitation occurs at cavitation numbers σ_T near 0.6, bursts of cavitation occur at 0.3, which begin to cause damage to surfaces. As the number increases, cavitation still may exist, but the bubble dynamics—i.e., size, internal pressure, and periodicity of formation–collapse–reformation—will be different.

Experiments in the CaviMax to characterize the fluid flow varied the orifice size in the single-orifice processor from 1.75 to 6 mm (orifice removed). As mentioned before, the instrument operates at constant flow; thus, the pressure of the measurement decreases as the applied orifice size increases. The flow measurements using this processor resulted in the ability to vary Reynolds numbers between 60,000 and up to 175,000, whereas the range of the available throat cavitation number was 0.85 to 1.7.

In subsequent metal oxide synthesis experiments, the relationship between cavitation numbers and Reynolds numbers to synthesis results, such as crystallographic strain, primary grain size, agglomerate size, or phase purity, was examined to develop an understanding of the effects of different bubble dynamics on crystal properties.

D. Synthesis of Metal Oxide Catalysts and Supported Metals by Hydrodynamic Cavitation

Using the synthetic strategy described previously and depicted in Fig. 3, hydrodynamic cavitation catalyst synthesis experiments were carried out using the continuous-flow system shown in Fig. 5. Two burettes are shown at the left of the figure. Normally only one burette is needed because many syntheses may be carried out by dissolving all the required metal salts in a single solution. However, when salt solutions are incompatible—e.g., one or more components precipitate when mixed—then two or more burettes are required, and in this case, the two solutions containing the different salts are metered into the system at a rate required to achieve the desired stoichiometry. The salt solution is then contacted with a precipitating agent such as aqueous solutions of ammonium carbonate, ammonium hydroxide, metal hydroxides or even a solvent in which all the metal ion components are insoluble. At this point the cavitation processor is in full operation, and the precipitating agent is circulating from the reservoir through the cavitation zone and back to the reservoir. The metal salt solution contacts the precipitating agent at the very bottom of the reservoir; all components immediately precipitate, and the slurry is drawn directly into the high-pressure zone, where the pressure is elevated to the desired head pressure. The set head pressure and orifice set selection determine the Reynolds number and throat cavitation number for the synthesis. The effluent from the cavitation chamber is normally recycled back to the reservoir, but this is done only to achieve the maximum possible effect. Several systems examined showed no difference between a one-pass-through experiment and a recycle one. For commercial operations requiring high throughput, the single-pass mode would be used in most cases. In the recycle mode, the metal salt addition is usually done over 20 min, and another 10 min is allowed for total recycle. After synthesis, the solids are either isolated by high-rpm centrifuging or pressure filtration in 1-liter stainless steel filters equipped with a 0.2-μm nylon filter. All solids were dried at 298 K for at least 12 h. Depending on the system, X-ray diffraction, transmission electron microscopy, and X-ray photoelectron spectroscopy were measured on either the dried samples or samples that had been calcined in air to different temperatures.

E. Estimation of the *in Situ* Calcination Temperature in MoO_3 Synthesis

An important aspect of materials synthesis by hydrodynamic cavitation is the degree of *in situ* calcination of the sample while it is flowing in a liquid medium in a high-shear environment. To estimate this heating, the synthesis of MoO_3 was investigated using several cavitational conditions and both processors. These results were compared to the synthesis by simply heating the starting material, ammonium heptamolybdate, $(NH_4)_6MoO_7 \cdot 7H_2O$, to eight different temperatures from 373 up to 598 K in a calcining oven in air for 4 h. When the ammonium molybdate is heated to different temperature levels, several different intermediates are generated, whose phases are well characterized in the literature. To estimate the average bulk temperature to which the solids are heated for the extremely short residence times in the flowing stream through the cavitation generator, the cavitation processed materials were air-dried at 373 K and their phase composition was compared with those of the oven-prepared materials at the different temperatures. To approximate the oven preparation in the cavitation processor, the ammonium molybdate was dissolved in a small amount of water and fed into a large volume of isopropanol, which contained a low concentration of ammonium hydroxide (0.03 *M*) to ensure complete precipitation. The precipitation technique was used rather than simply passing a slurry of the insoluble crystals through the processor to better simulate the grain size of processed insoluble material and the bubble size defined by the process conditions. A variety of cavitation conditions were studied in both the CaviPro 300 and CaviMax processors. After the cavitation synthesis, the solid materials were filtered and air-dried at 373 K, the XRD was measured, and a complete phase analysis was made on each similarly treated sample. A complete phase analysis was performed on all the oven-calcined samples at the different temperatures. The latter analysis provided information on the composition of the different species resulting from a 4-h calcination for comparison to the cavitation processed samples, which had been dried at 373 K. In addition, kinetic data were obtained for the decomposition of one of the stable intermediates because it appeared in the XRD from samples at several temperatures. These reactivity data at different temperatures were used to qualitatively evaluate the activation energy for the decomposition of the oven-calcined samples. This activation energy was then applied in the Arrhenius equation, along with the residence time of the fluid element inside the cavitation section (recovery zone) to determine short-lived *in situ* heat-up temperature from the shock wave. The effective bulk temperature of *in situ* heating of the particles in the cavitation experiments was obtained by comparing the phase observed after the 373 K drying to the temperature required to give

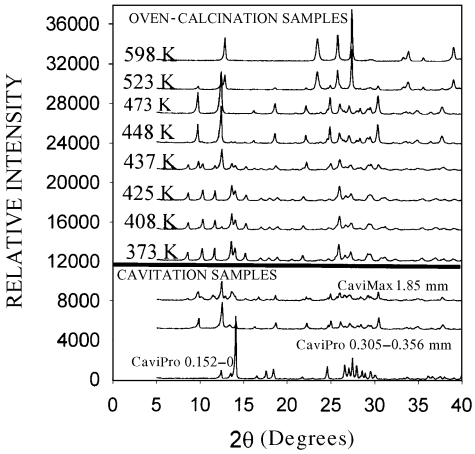

FIG. 6. XRD analysis of oven-calcined ammonium molybdate for 4 h at progressively higher temperatures are shown in the top half of the figure. The XRD of 373 K–dried products from the treatment of ammonium molybdate in an inert solvent in the CaviPro 300 and CaviMax processors are shown in the bottom half of the figure.

the same phase in the oven-calcined series. Three cavitation-prepared samples were compared to the eight oven-calcined samples in Fig. 6 by XRD. The top eight diffraction patterns resulted from the oven calcinations to the temperatures indicated on the graph. The lower three patterns resulted from processing ammonium molybdate using the CaviPro equipped with a 0.152-mm orifice in the first (upstream) position and no orifice in the second position. Also, the XRD of the cavitation sample processed with the orifice set 0.305–0.356 mm is displayed along with a CaviMax experiment that used the 1.85-mm orifice. After cavitational processing, all the samples were dried at 373 K and analyzed by XRD.

The sample obtained from the lowest temperature oven calcination at 373 K was identified as having a main phase of $(NH_4)_8Mo_{10}O_{34}$, N/Mo = 0.8 (ICDD, 1997b). In the oven-calcined series, the 473 K sample was identified as having a main phase of $(MoO_3)_4(NH_3)_2(H_2O)$, N/Mo = 0.5, according to the ICDD data base (ICDD, 1997c). The cavitation processed sample using the single 0.152-mm orifice and dried at 373 K was identified as triclinic ammonium molybdenum oxide $(NH_4)_4Mo_8O_{26}$, N/Mo = 0.5 (ICDD, 1997a). The composition of the oven-calcined sample at 473 K for 4 h had the same composition as the CaviPro sample processed for short residence times; namely, the N/Mo ratios for both were 0.5 and the O/Mo ratios were 3.25. Thus, their compositions are the same and their crystallographic structures are very similar, with the triclinic phase resulting from the cavitation treatment likely being of slightly higher energy. From these data, we conclude

that the effective average bulk temperature resulting from the shock wave heating was approximately 473 K. For the CaviPro sample processed using the dual orifice set 0.305–0.356 mm, the estimated average bulk temperature heating was around 448 K, and processing in the CaviMax using the single 1.85-mm orifice resulted in an effective heating to 438 K.

Using the approximate phase composition data obtained from the 425, 437, 448, and 473 K oven-calcined samples in the middle section of Fig. 6 and assuming a first-order solid-state decomposition of ammonium molybdate, an activation energy of around 92 kJ/mol was computed. In the CaviPro synthesis, the number of recycles was 4.16 passes of the 600-ml solution flowing at a rate of 125 ml/min through the cavitation chamber. Because the volume between the two orifices was 0.20 ml (in the recovery zone), the total contact time for the ammonium molybdate solution was 0.385 s in the recovery zone. Using the oven-calcination experiment at 473 K, where the conversion to the $(MoO_3)_4(NH_3)_2(H_2O)$ intermediate phase was at least 95%, assuming first-order kinetics and a total reaction time of 4 h results in a first-order rate constant of 1.599×10^{-4} s^{-1}. Because the degree of conversion to an intermediate of the same stoichiometry, $(NH_4)_4Mo_8O_{26}$, was obtained from the cavitation experiment, a first-order rate constant of 0.385 s^{-1} was calculated, assuming that all the shock wave heating occurred within the 0.20-ml reaction zone between the orifices and that the reaction maintains the same order—i.e., first order, as in the oven-heated samples of ammonium molybdate. Applying these rate data to the Arrhenius equation and making the calculation assuming that the preexponential factor and activation energies are the same for both reactions, the effective *in situ* shock wave average heat-up temperature that the gel particles experience is around 700 K. Naturally, the temperature of the shock wave would be much higher than this number, but average effective heat transferred corresponds to heating the particle to 700 K. This estimate is regarded as conservative because the time constant for bubble collapse–reformation–collapse is likely much less than the residence time computed using the volume of the cavity. Thus, a more realistic residence time to use in the first-order kinetic treatment would be the time constant for the shock wave interacting with each solution element. As a limit in calculating the minimum *in situ* heat-up temperature, the velocity of sound through liquid water at 298 K was used in combination with the solution volume and the 4.16 recycle passes to compute the first-order rate constant. Calculation of the reaction rate based on these data and applying the rate to the Arrhenius equation resulted in an average *in situ* shock wave transient heat-up temperature of 950 K. These values for the *in situ* heat-up temperature should not be compared to the values of 2000 to 5000 K reported by Suslick and co-workers for the heat-up temperatures within the bubble resulting from acoustic cavitation (McNamara *et al.,* 1999; Suslick, 1993;

Suslick, *et al.,* 1999a). Cavitational heating results from heating within the bubble and shock wave heating. Heating within the bubble is regarded as ineffective for heating components located outside the bubble, whereas shock wave heating is responsible for heating components within a few radii of the bubble. Thus, we conclude that the effective shock wave *in situ* calcination temperature lasting for very short heating times is in the range of 700 to 950 K, and this will vary, depending on the metal oxide being synthesized due to the differences in heat-transfer coefficients for the metal oxide gel component.

A second method for acquiring evidence for shock wave heating was gained from passing a screened sample of calcium fluoride, CaF_2, through a CaviMax processor in water and recirculating for 30 min. The scanning electron micrograph of the untreated CaF_2 is shown in Fig. 7, and the CaviMax-processed sample is shown in Fig. 8. The melting point of CaF_2 is 1360°C. A comparison of the SEM of the cavitation-processed sample and unprocessed sample shows that the processed sample in Fig. 8 contained mainly CaF_2 crystals, which were rounded off, and many particles were attached to one another by melted necks. This suggests that the particles were heated to a sufficiently high temperature so that a major fraction of the particle's

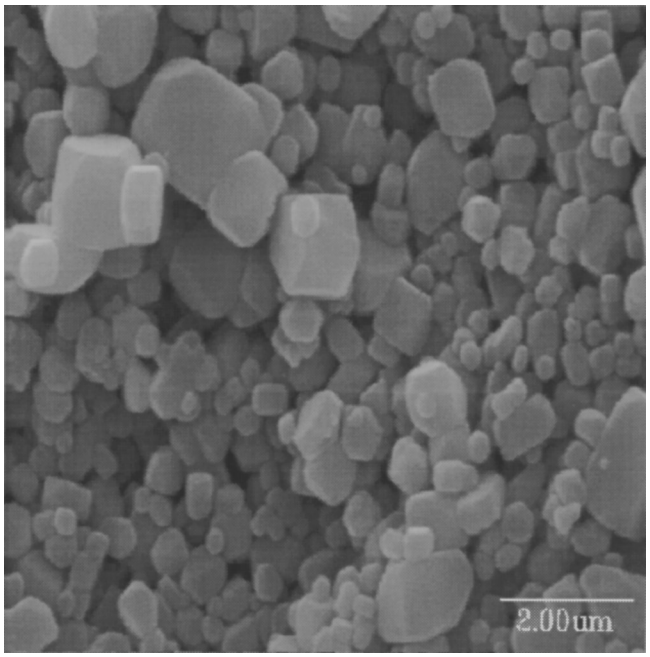

FIG. 7. A sample of calcium fluoride (CaF_2) that had been ground and screened to approximately 2 μm.

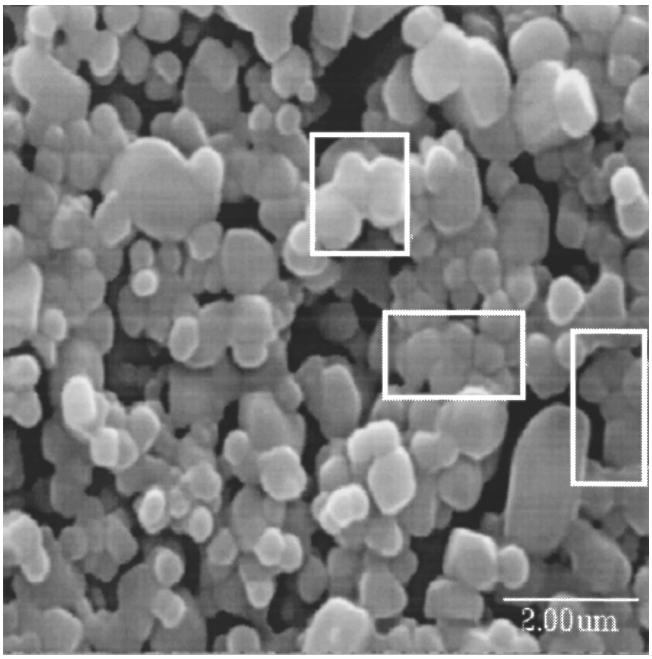

FIG. 8. A sample of the CaF_2 that had been screened to 2 μm (seen in the SEM in Fig. 7) which was processed in the CaviMax processor with recirculation as a slurry in water for 30 min. The highlighted areas indicate particles having melted necks.

surface had melted or at least softened. One can expect that CaF_2 would soften at the Tamman temperature of about 50% of its normal melting point. Thus, a shock wave heat-up temperature to about 600°C is consistent with the data for ammonium molybdate decomposition. These results are similar to those observed (Suslick, 1993) for shock wave heating in ultrasound experiments, where similar melting was observed after high-melting solids were processed in an acoustic cavitational stream.

F. Hydrodynamic Cavitation Synthesis of Nanostructured Catalysts in High-Phase Purities and Varying Grain Sizes

One of the advantages of cavitational synthesis, providing the synthesis equipment has the capability to adjust the bubble dynamics, is the capability to do synthesis under the conditions of both high shear and *in situ* calcination. If the equipment can be adjusted to operate in slightly different fluid dynamic regimes, it should be possible to obtain both high-phase purity catalysts and to systematically adjust the primary grain size of the crystallites

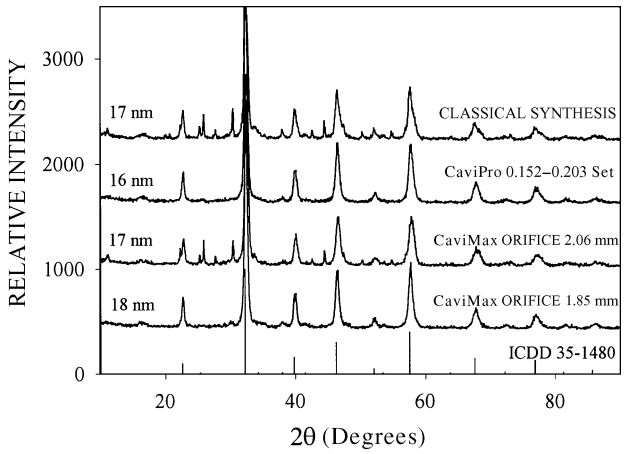

FIG. 9. XRD of the CaviMax and CaviPro 300 synthesis of $La_{0.6}Sr_{0.4}FeO_3$ compared to the classical synthesis.

in the important region of 1 to 20 nm. Syntheses of several complex metal oxide systems were studied in order to determine whether hydrodynamic cavitation had the capabilities to meet the previously mentioned synthetic objectives.

The synthesis of β-$Bi_2Mo_2O_{12}$ (β-bismuth molybdate) and a multimetallic perovskite, $La_{0.6}Sr_{0.4}FeO_3$, were examined to determine whether the cavitational synthesis afforded both superior phase purities and variable grain sizes, as contrasted with classical methods of coprecipitation synthesis. The perovskite synthesis was extensively examined in the CaviPro 300 and the CaviMax using a variety of different orifice sets to intentionally vary the bubble dynamics. In all cases, the products were isolated by filtration and calcined to different temperatures for 12 h, after which their grain sizes and phase purities were examined by XRD. The XRD patterns in Fig. 9 resulted from catalysts synthesized in the CaviMax processor using the 1.85-mm orifice (lowest curve) and the 2.06-mm orifice (second curve from the bottom). The CaviPro 300 processor was used with several different orifice sets, and the XRD resulting from the 0.152-mm (first orifice) and 0.203-mm (second orifice) set is illustrated in the third curve from the bottom. For comparison purposes, the XRD of a coprecipitation carried out under conditions of high-speed mechanical mixing with the identical chemistry and precipitation technique is illustrated in the top diffraction pattern in the figure. All materials in the figure were calcined to 873 K for 12 h after synthesis. The XRD data show that the two CaviMax synthesized materials gave substantially different results; namely, the smallest orifice size, 1.85 mm, resulted in both very high phase impurity and a grain size of 18 nm, whereas the 2.06-mm

orifice afforded a material having substantial amounts of impure phases in a grain size of 17 nm. Synthesis using the 2.26- and 2.43-mm orifices in two other CaviMax experiments resulted in the same low degree of phase impurity as observed using the 2.06 orifice, and the grain sizes were 17 and 16 nm, respectively. However, synthesis using the CaviPro 300 processor resulted in high-phase pure materials for all experiments using a constant size for the first orifice while varying the size of the downstream orifice. The orifice sets studied were 0.152–0.203, 0.152–0.254, 0.152–0.305, and 0.152–0.356. The XRD data using the 0.152–0.203 sets are illustrated in the third curve from the bottom of Fig. 9. The XRD data for the classically prepared material are illustrated in the top curve in the figure, and this pattern shows that large amounts of separate phase compounds were observed in the sample. The grain size of the CaviPro 300–prepared materials was 16 nm, whereas the classical was 17, and the grain sizes resulting from all four of the orifice sets studied were between 16 and 18 nm. Thus, although the cavitational synthesis resulted in high phase purities and the classical synthesis did not, the fluid dynamic region studied was not able to systematically vary the grain size of the calcined materials.

The synthesis of β-$Bi_2Mo_2O_{12}$ using both the CaviMax processors afforded results that paralleled those of the perovskite synthesis. The phase purity of the catalysts after calcination at 623 K by cavitation using the 1.85-mm orifice gave phase-pure $Bi_2Mo_2O_{12}$, whereas the parallel classical synthesis contained a modest amount of the alpha phase. Processing using the 2.06-, 2.26-, and 2.41-mm orifices all resulted in a modest amount of impure phase similar to the classical synthesis and grain sizes after 623 K calcination of 22, 28, and 21 nm, respectively. The grain size observed using the 1.85-mm orifice was 11 nm, whereas the classical synthesis resulted in 19 nm.

G. The Introduction of Crystallographic Strain in Catalysts by Hydrodynamic Cavitation

During our studies on hydrodynamic cavitation-mediated catalyst synthesis, we observed the introduction of crystallographic strain in several metal oxide systems. As the size of a crystallite decreases into the range of a few nanometers, both crystallographic strain and defects in metal oxides increase, and it was shown that higher defect concentrations in metal sulfides result in higher HDS catalytic reactivity (Mdleleni *et al.,* 1998). The degree of strain in nanostructured materials synthesized by cavitation was characterized by the Williamson–Hall XRD (Williamson and Hall, 1953) technique. The strain induced during cavitational synthesis was investigated for titania, several piezoelectric (PZT) systems in the family $PbZr_xTi_{1-x}O_3$, and the synthesis of an alumina-stabilized copper-modified zinc oxide. A wide variety

of fluid dynamic conditions were investigated to understand the relationship between strain and cavitation. The expectation was that as the primary grain size decreased, the strain would increase. After collection of the data for the titania and PZT, a classical engineering technique, the Buckingham (1914) pi theorem was applied to the systems for predicting flow regimes that result in the highest degree of crystallographic strain.

1. Titania

Because strain in nanostructured titania should affect both the electronic and catalytic properties of the materials, an extensive study of the cavitational synthesis of titania was carried out. The synthesis of titania starting with titanium butoxide, precipitated in either pure water or using stoichiometric to various excess amounts of water in isopropanol, was studied in both the double-orifice processor (CaviPro 300) and the single-orifice processor (CaviMax). The syntheses in the single-orifice processor were carried out in pure water by running a 0.5 *M* solution of the butoxide in isopropanol into a recirculation stream of water. The XRD analysis of these materials after calcination at 673 K showed an unusual degree of induction of crystallographic strain as compared to the materials prepared by classical precipitation, and the amount of strain depended on the fluid dynamic conditions applied in the synthesis. The XRD data for titania synthesis using the single-orifice processor equipped with six different orifice diameters from 1.85 to 1.92 mm are shown in Fig. 10. Included in the figure are the grain sizes observed after a 673 K calcination. Although the Reynolds numbers and throat cavitation numbers were varied over a wide range, the primary grain sizes were nearly constant. However, the strain systematically increased up to 0.34%, which is much higher than the classically prepared material of 0.25% with a grain size

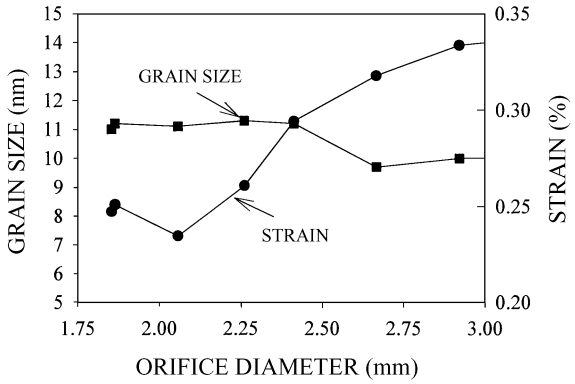

FIG. 10. Grain size and crystallographic strain data for the synthesis of titania using the CaviMax processor as a function of different orifice sizes used in the processor.

of 14 nm compared to the 11-nm grains in the cavitation experiments. Using the smallest orifice shown in Fig. 10 (1.85 mm), several syntheses were carried out where titanium butoxide in isopropanol was reacted with a circulating solution of water in stoichiometric amounts up to 16 times the stoichiometric ratio. These syntheses resulted in slightly lower strain, near 0.25%, whereas the classical preparations afforded strains of 0.20% and grains of 15 nm. Synthesis in the two-orifice processor using a downstream constant orifice size of 0.356 mm while the first orifice was varied in four ranges from 0.178 to 0.305 mm resulted in a substantially higher strain of 0.55% and slightly smaller grain sizes of 10 nm. The grain sizes were constant irrespective of the size of the first orifice, whereas the strain was highest using the smallest first orifice.

It is clear from the preceding results that cavitational synthesis generates substantially more strain in the titania crystallite than classical synthesis and that the high-pressure experiment (dual-orifice processor) introduces more than the low-pressure synthesis. Furthermore, the amount of strain can be systematically varied by changing the processor's operating parameters. To aid in understanding the relationship between the fluid-flow properties of the cavitational synthesis and the degree of strain induced in the titania synthesis, a Buckingham (1914) pi treatment was applied to the titania synthesis data obtained from the single-orifice processor. This dimensional analysis of the pertinent dimensionless variables (Find *et al.,* 2000) resulted in a three-dimensional surface with a correlation coefficient of 0.92, as shown in Fig. 11.

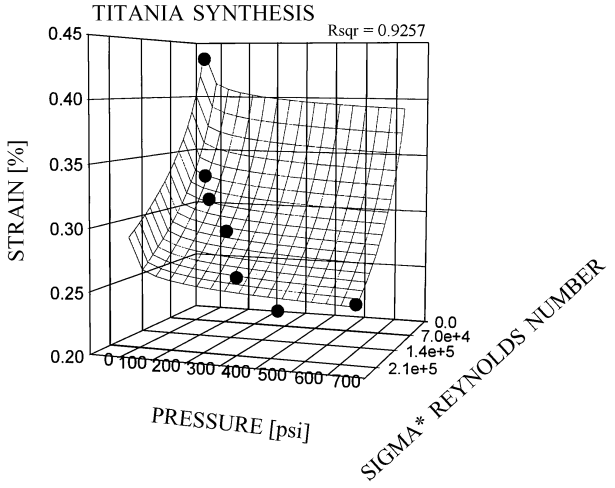

FIG. 11. Three-dimensional surface plot showing the correlation of applied pressure, crystallographic strain, and Reynolds number–throat cavitation number for the synthesis of titania using the CaviMax processor.

After the analysis was completed, the plot was used to predict the processor conditions required to synthesize the point of highest strain in the figure of 0.44%. A power law fit of the data showed that the microstrain was more sensitive to changes in the Reynolds number, but the strain decreased as the Reynolds number increased. Over the regime studied, the microstrain increased as the cavitation number decreased for $\sigma_T = 0.5$ to 1.8.

A series of experiments were carried out to determine whether cavitational processing of a preformed nanostructured titania could further reduce the primary grain size and reduce the agglomerate size. For this experiment a sample of titania previously calcined to 673 K was recirculated through the dual-orifice processor using the 0.254–0.356 orifice set at a constant pressure of 120 MPa in two experiments, one in water and the other in *n*-hexane. Each system was studied over 4 h of processing, the starting titania was sieved to agglomerates of greater than 1000 nm, and the primary grain size was 13 nm. In the case of the water system, after 1 h, 65% of the agglomerated particles had been reduced to below 1000 nm and the distribution was centered at 600 nm. After 3 h, 72% of the agglomerates had been reduced to below 1000 nm, with agglomerates centered at 300 nm. Processing in hexane resulted in 74% agglomerates below 1000 nm after 1 h, with the distribution centered at 300 nm. After 4 h 88% of the particles were below 1000 nm, and the distribution was bimodal (centered at 150 nm and 500 nm). The grain size of the titania remained unchanged from the original 13 nm after any of the processing. An interesting feature of the materials processed in water is that the XRD intensities of the anatase peaks linearly decreased with processing time to 50% of their original intensity after 4 h. Because the grain size did not change and the background (indicating amorphous materials) did not change very much, we conclude that the decline in intensity was due to a lower materials density of the processed solids. After the initial processing time, the microstrain increased linearly with increased processing time, and the amount of rutile in the sample systematically increased from 0 to 10%.

2. Piezoelectrics

A wide range of studies in the single- (CaviMax) and double-orifice processors (CaviPro 300) on the piezoelectric (PZT) system in the family $PbZr_xTi_{1-x}O_3$ showed that the processing parameters could greatly enhance the amount of microstrain to values as large as 0.93%. Figure 12 illustrates the range of microstrain that resulted from cavitational processing in both the single-orifice and double-orifice processors. The microstrain was measured on samples calcined in air at 873 K. The figure shows that the high-flow-rate, single-orifice processor resulted in a much higher degree of induced strain than the low-flow, high-pressure single-orifice processor. In the figure, the

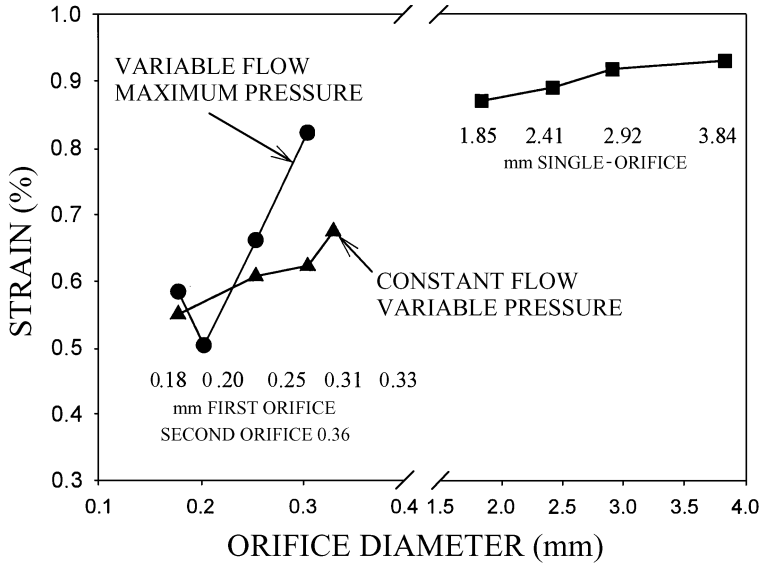

FIG. 12. Strain introduced into PZT crystallites of $PbZr_{0.5}Ti_{0.5}O_3$ by cavitational processing in the double-orifice processor (CaviPro 300) as a function of different sets of orifices, shown on the left side of the figure. Similar data using the single orifice processor (CaviMax) are shown on the right side of the figure.

range of minimum to maximum pressure for the double-orifice, variable-flow, maximum-pressure experiments was 20.6 to 169 MPa. The flow rate in the constant-flow, variable-pressure experiments used constant flow rates of 400 ml/min by adjusting the operating pressure of the processor. Other experiments showed that all the cavitational synthesized PZT compositions were essentially 100% pure phase, whereas the classically prepared materials all contained modest amounts of secondary phases. The grain sizes of the cavitational samples after 873 K air calcination were around 25 nm. Although it has not been reported experimentally in the literature, it would be expected that these high levels of microstrain would affect both the piezoelectric properties and the rates of grain growth.

3. Copper-Modified Zinc Oxide

Several series of methanol synthesis catalysts were prepared by the co-precipitation of the appropriate metal salts in either Na_2CO_3 or $(NH_4)_2CO_3$ using the CaviPro 300 (dual-orifice processor) at both high and low pressures. The experiments were carried out using a 0.152-mm first orifice while varying

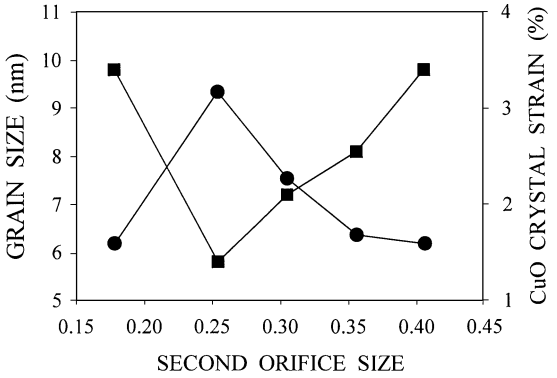

FIG. 13. Grain sizes and crystallographic strain in CuO after 623 K calcination of $Cu_{0.22}Zn_{0.68}Al_{0.10}$ catalysts from a CaviPro 300 synthesis using a 0.152-mm first orifice while varying the second orifice between 0.178 and 0.406 mm. The composition of the catalyst was $Cu_{0.22}Zn_{0.68}Al_{0.10}$.

the second orifice between 0.178 and 0.406 mm at a constant head pressure of 138 MPa. The resulting catalysts had the composition of $Cu_{0.22}Zn_{0.68}Al_{0.10}$ and were calcined at 623 K in air before XRD analysis to determine both the crystallographic strain and the grain size of the CuO component. A similar analysis was performed on the ZnO component, but both the grain sizes and the strain were essentially constant as a function of the orifice set applied in the synthesis. However, both the grain size and the strain of the CuO component varied as the orifice size of the second orifice was varied. Figure 13 illustrates that the cavitational synthesis results in the capability to systematically vary not only the grain size of the CuO component, but also the crystallographic strain. The strain increased as the grain size of the CuO decreased. In view of the report (Doesburg *et al.,* 1987) that methanol synthesis rates using nanometer-sized CuO catalysts varied according to the grain size, this ability to systematically vary the CuO grain size is likely important for the synthesis of catalysts having the appropriate grain size corresponding to the highest catalytic rates of methanol formation.

H. SYNTHESIS UNDER VARIABLE FLUID-FLOW CONDITIONS

By a simple mechanical adjustment in the orifice sizes, type of processor, or the head pressure, the cavitation bubble dynamics can be systematically altered. When catalyst synthesis is carried out under different conditions obtained by this type of adjustment, the structures and grain sizes of products

vary considerably. This section gives a few examples of the divergent synthesis results for a few of the materials that were synthesized.

1. Synthesis of High-Temperature Stable Oxidation Catalysts

The synthesis of catalysts for high-temperature gas turbine applications was carried out to obtain a 2% w/w Pd on zirconia–alumina. The synthesis used 5 mol% alumina as a stabilizer to prevent grain growth of the zirconia support. In this synthesis, all components were precipitated in a single step using the CaviMax processor equipped with the 1.85-, 2.06-, 2.41-, or 2.92-mm orifice. The products after filtration, drying, and calcination to 1373 K were analyzed by XRD; the diffraction patterns are illustrated in Fig. 14. A classical experiment was carried out using rapid mechanical stirring in the precipitation step and is illustrated in the top diffraction pattern of the figure. It is interesting to note that these conditions resulted in the formation of mainly the monoclinic phase of zirconia in the classical preparation. The cavitational preparation formed mainly this same phase using the smallest orifice (1.85 mm), but as the orifice size increased up to 2.92 mm, the calcined materials were mainly a cubic zirconia containing a small amount of the monoclinic phase. Although the Pd reflection at 40.25° 2θ is weak in all cases, it can be seen from the figure that the reflection grew when the 2.92-mm orifice was used. Quantification of the grain sizes was performed using long analysis times and showed that the 2.41-mm experiment

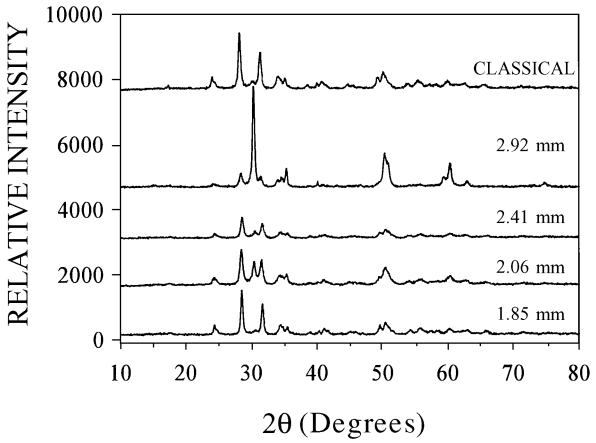

FIG. 14. XRD results for the synthesis of 2% Pd on zirconia–5 mol% alumina after 1373 K calcination using the CaviMax processor equipped with either the 1.85-, 2.06-, 2.41-, or 2.92-mm orifice. The corresponding classical preparation is illustrated at the top of the figure.

resulted in a Pd grain size of 36 nm, whereas the Pd grain size in the 2.92-mm orifice experiment was about 100 nm.

2. Synthesis of Variable Phases under Different Bubble Dynamics

The synthesis of 2% Ag on alumina was studied in both the CaviMax and CaviPro 300 processors under a wide variety of bubble dynamic conditions. Several catalysts were synthesized by a single-step precipitation of both the metal and the alumina support, which passed into the high-pressure pump of the processor. In the CaviPro 300, the orifice sets 0.127 mm/0.356 mm, 0.178 mm/0.356 mm, 0.229 mm/0.356 mm, and 0.279 mm/0.356 mm were studied in recycle experiments. After the products were dried at 298 K overnight, the XRD of the catalysts showed that when the smallest first orifice in the set, 0.127 mm/0.356 mm, was used, the product was nearly pure Böhmite, whereas using progressively larger first-orifice diameters, as in the 0.178 mm/0.356 mm experiment, resulted in mainly Bayerite. The XRD analysis on these materials is shown in Fig. 15. A similar set of experiments using different orifices sizes in the CaviMax single-orifice processor resulted in a similar variability in alumina structure. In all cases, the silver grains were very small, as seen by inspecting the weak reflections near 64° 2θ. The material from the experiment that afforded mainly Bayerite was transformed to η-Al_2O_3 when air-calcined to 673 K and θ-Al_2O_3 when calcined to 1073 K. The material exhibiting mainly Böhmite reflections was transformed to γ-Al_2O_3 upon calcination to 673 K and δ-Al_2O_3 when calcined to 1073 K. Thus, this type of synthesis has the capability of affording nanostructured

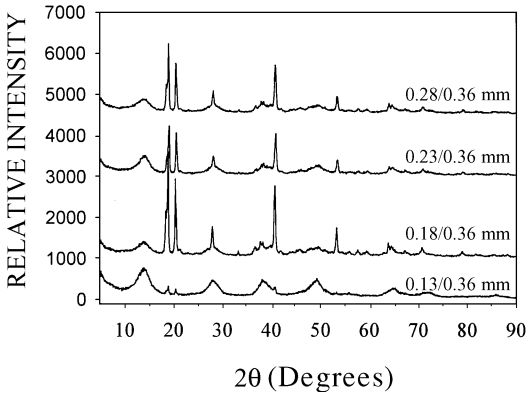

FIG. 15. XRD diffraction patterns for the synthesis of Ag 2% w/w on alumina after drying at 373 K. The catalysts were obtained from processing in the CaviPro 300 using the orifice sets 0.127 mm/0.356 mm, 0.178 mm/0.356 mm, 0.229 mm/0.356 mm, and 0.279 mm/0.356 mm.

grains of Ag supported on nanometer-size grains of various transitional aluminas by conducting the synthesis under different hydrodynamic cavitation conditions.

V. Conclusions

A large number of novel techniques for the synthesis of nanostructured materials have been developed in recent years. Most of the processes rely on either chemical techniques or mediated synthesis by polymers or surfactants to produce nanostructured grains of catalyst that are stable. Few processes result in the general ability to systematically vary the primary crystallite grain sizes in the important range 1–20 nm, which is critical for the discovery of active and selective catalysts. Many processes result in the formation of multimetallic catalysts in high phase purities, which is just as important for catalysis. Hydrodynamic cavitation processing affords the capability to calcine precipitated products during the synthesis step and to systematically introduce crystallographic strain. In some cases, the hydrodynamic cavitation process afforded variable catalyst grain sizes in the range 1–10 nm by a simple mechanical adjustment in the process parameters, but metal oxide synthesis did not generally result in a large variability of grain sizes.

ACKNOWLEDGMENTS

We thank Five Star Technologies of Cleveland, Ohio, for generous financial support of this research. We also acknowledge Soonan Nguyen, Tri Giang, Vinh Voduc, and Hieu Nguyen for their help in some syntheses and XRD analyses.

REFERENCES

Allpress, J. G., and Sanders, J. V., Structure and stability of small clusters of atoms. *Aust. J. Phys.* **23,** 23 (1970).

Baetzold, R. C., Calculated properties of metal aggregates. I. Diatomic molecules. *J. Chem. Phys.* **55,** 4355 (1971).

Baetzold, R. C., Molecular orbital description of catalysis by metal clusters. *J. Catal.* **29,** 129 (1973).

Behrens, S., Dinjus, E., and Unger, E., Protein supported metallic nanostructures. *Nachrichten (A publication of the Forschungszentrum Karlsruhe, Germany),* **31,** 117 (1999).

Behrens, S., Habicht, W., Boukis, N., Dinjus, E., Baum, M., and Unger, E., Private communication from S. Behrens, Institut fur Technische Chemie, Forschungszentrum Karlsruhe, Germany (2000).

Berthet, A., Thomann, A. L., Aires, F. J. C. S., Brun, M., Deranlot, C., Bertolini, J. C., Rozenbaum, J. P., Brault, P., and Andrezza, P., Comparison of bulk Pd/(Bulk SiC) catalysts prepared by atomic beam deposition and plasma sputtering decomposition: Characterization and catalytic properties. *J. Catal.* **190,** 49 (2000).

Birringer, R., Gleiter, H., Klein, H. P., and Marquardt, P., Nanocrystalline materials—An approach to a novel solid structure with gas-like disorder. *Phys. Lett. A* **102,** 365 (1984).

Brennan, C. E., "Cavitation and Bubble Dynamics." Oxford Univ. Press, New York (1995).

Buckingham, E., On physically similar systems: Illustrations of the use of dimensional equations. *Phys. Rev.* **4,** 345 (1914).

Busser, G. W., van Ommen, J. G., and Lercher, J. A., Preparation and characterization of polymer-stabilized rhodium particles, *in* "Advanced Catalysts and Nanostructured Materials, Modern Synthetic Methods" (W. R. Moser, Ed.), p. 213. Academic Press, San Diego (1996).

Cox, D. M., Kaldor, A., Fayet, P., Eberhardt, W., Brickman, R., Sherwood, R., Fu, Z., and Sondericher, D., Effect of cluster size on chemical and electronic properties, *in* "Novel Materials in Heterogeneous Catalysis" (R. T. K. Baker and L. L. Murrell, Eds.), Vol. 437, p. 172. Amer. Chem. Soc. Symp. Ser. Washington, DC (1990).

Crooks, R. M., Zhao, M., Sun, L., Chechik, V., Yeung, L. K., and Lemon, B. I., Dendrimer-encapsulated nanoparticles: Synthesis, characterization, and applications to catalysis, private communication.

de Heer, W. A., The physics of simple metal clusters: Experimental aspects and simple models, *Rev. Modern Phys.* **65**(3), 612 (1993).

Del Vallee, M., Avalos-Borja, M., Cruz, J., and Fuentes, S., Molecularly designed ultrafine/nanostructured materials, *Mater. Res. Soc, Symp. Proc.* **351,** 287 (1994).

Dhas, N. A., and Gedanken, A., Characterization of sonochemically prepared unsupported and silica supported nanostructured pentavalent molybdenum oxide, *J. Phys. Chem. B* **101,** 9495 (1997a).

Dhas, N. A., and Gedanken, A., Sonochemical synthesis of molybdenum oxide—and molybdenum carbide–silica nanocomposites. *Chem. Mater.* **9,** 3144 (1997b).

Dhas, N. A., Cohen, H., and Gedanken, A., *In situ* preparation of amorphous carbon-activated palladium nanoparticles. *J. Phys Chem. B* **101,** 6834 (1997a).

Dhas, N. A., Koltypin, Y., and Gedanken, A., Sonochemical preparation and characterization of ultrafine chromium oxide and manganese oxide powders. *Chem. Mater.* **9,** 3159 (1997b).

Ding, J. H., and Gin, D. L., Catalytic Pd nanoparticles synthesized using a lyotropic liquid crystal polymer template, *Chem. Mater.* **12,** 22 (2000).

Doesburg, E. B. M., Hoppener, R. H., de Koning, B., Xiaoding, X., and Scholten, J. J. F., Preparation and characterization of copper/zinc oxide/alumina catalysts for methanol synthesis, *in* "Preparation of Catalysts IV" (G. Poncelet, J. Martens, B. Delmon, P. A. Jacobs, and P. Grange, Eds.), pp. 31, 767. Elsevier, Amsterdam (1987).

Ebner, K., Process and Apparatus for the Thermal Decomposition of Substances or Mixtures of Same, U.S. Patent 2,155,119, Assigned to American Lurgi Corporation (April 18, 1939).

Ebner, K., Process and Apparatus for the Thermal Decomposition of Substances or Mixtures of Same, West German Patent 753,306, Assigned to American Lurgi (1951).

Ebner, K., Thermal Decomposition of Substances, West German Patent 877,196, Assigned to American Lurgi (1953).

Emerson, S. C., Coote, C. F., Booth, H., Tufts, J. C., LaRocque, R., and Moser, W. R., The ultrasonic synthesis of nanostructured metal oxide catalysts, *in* "Studies in Surface Science and Catalysis" (G. Poncelet, J. Martens, B. Delmon, P. A. Jacobs, and P. Grange, Eds.), pp. 118, 773 (1998).

Find, J., Emerson, S. C., Krausz, I. M., and Moser, W. R., Hydrodynamic cavitation as a tool to control, macro-, micro-, and nano-properties of inorganic materials, *J. Mater. Res.* (2001).

Fuentes, S., and Figueras, F., The influence of particle size on the catalytic properties of alumina-supported rhodium catalysts. *J. Catal.* **61,** 443 (1980).

Gleiter, H., *in* "Deformation of Polycrystals: Mechanism and Microstructure" (N. Hansen, A. Horsewell, T. Leffers, and H. Lilholt, Eds.), **15,** Riso National Laboratory, Rackilde, Denmark (1981).

Gleiter, H., Nanocrystalline materials. *Prog. Mater. Sci.* **33,** 223 (1989).

Grinstaff, M. W., Cichowlas, A. A., Choe, S. B., and Suslick, K. S., Effect of cavitation conditions on amorphous metal synthesis. *Ultrasonics* **30,** 168 (1992).

Haruta, M., Size- and support-dependency in the catalysis of gold. *Catal. Today* **36,** 153 (1997).

Haruta, M., Tsubota, S., Kobayashi, T., Kageyama, H., Genet, M. J., and Delmon, B., Low temperature oxidation of CO over gold supported on titania, iron oxide, and cobalt oxide. *J. Catal.* **144,** 175 (1993).

Henry, C. R., Chapon, C., Giorgio, S., and Goyhenex, C., Size effects in heterogeneous catalysis: A surface science approach, *in* "Chemisorption and Reactivity on Supported Clusters and Thin Films," 331, 117, NATO ASI Ser., Ser. E, Dordrecht (1997).

Hyeon, T., Fang, M., and Suslick, K. S., Nanostructured molybdenum carbide: Sonochemical synthesis and catalytic properties, *J. Am. Chem. Soc.* **118,** 5492 (1996).

ICDD, *International Centre for Diffraction Data, Powder Diffraction File—2 Sets 1–47, Card 18–117* (1997a).

ICDD, *International Centre for Diffraction Data, Powder Diffraction File—2 Sets 1–47, Card 37–381* (1997b).

ICDD, *International Centre for Diffraction Data, Powder Diffraction File—2 Sets 1–47, Card 21–570* (1997c).

Jordan, M., Reznek, S. R., Neville, M. A., Soucy, B. A., and Mackay, B. E., High Surface Area Metal Oxide Foams and Method of Producing Same, U.S. Patent 4,937,062, Assigned to Cabot Corporation (June 26, 1990).

Kaldor, A., and Cox, D. M., Hydrogen chemisorption on gas-phase transition metal clusters. *J. Chem. Soc. Faraday Trans.* **86,** 2459 (1990).

Knapp, R. T., Daily, J. W., and Hammitt, F. G., "Cavitation", McGraw-Hill, New York. (1979).

Kozyuk, O. V., Method of obtaining free disperse system and device for effecting same, U.S. Patent 5,492,654, Exclusively Licensed to Five Star Technologies (Feb. 10, 1996).

Kozyuk, O. V., Method of Obtaining a Free Disperse System in Liquid and Device for Effecting the Same, U.S. Patent 5,810,052, Assigned to Five Star Technologies (Sept. 22, 1998).

Kozyuk, O. V., Method and Apparatus for Producing Ultra-thin Emulsions and Dispersions, U.S. Patent 5,931,771, Exclusively Licensed to Five Star Technologies (August 3, 1999a).

Kozyuk, O. V., Method and Apparatus For Conducting Sonochemical Reactions and Processes Using Hydrodynamic Cavitation, U.S. Patent 5,937,906, Exclusively Licensed to Five Star Technologies (August 17, 1999b).

Kozyuk, O. V., Method for Changing the Quantitative and Qualitative Composition of a Mixture of Liquid Hydrocarbons based on the Effects of Cavitation, U.S. Patent 5,969,207, Exclusively Licensed to Five Star Technologies (October 19, 1999c).

Kozyuk, O. V., Method and Apparatus of Producing Liquid Disperse Systems, U.S. Patent 5,971,601, Exclusively Licensed to Five Star Technologies (October 26, 1999d).

Kozyuk, O. V., Method and Apparatus For Conducting Sonochemical Reactions and Processes Using Hydrodynamic Cavitation, U.S. Patent 6,035,897, Exclusively Licensed to Five Star Technologies (March 14, 2000b).

Kozyuk, O. V., Method and Apparatus For Conducting Sonochemical Reactions and Processes Using Hydrodynamic Cavitation, U.S. Patent 6,012,492, Exclusively Licensed to Five Star Technologies (January 11, 2000a).

Li, S., Lee, J. S., Hyeon, T., and Suslick, K. S., Catalytic dehydronitrogenation of indole over molybdenum nitride and carbide with different structures. *Appl. Catal. A: General* **184,** 1 (1999).

Li, T., Moon, J., Morrone, A. A., Mecholsky, J. J., Talham, D. R., and Adatr, J. H., Preparation of Ag/SiO_2 nanosize composites by a reverse micelle and sol-gel technique. *Langmuir* **15,** 5328 (1999).

Martino, A., Kawola, J. S., Sault, A. G., Hampden-Smith, M., and Yamanaka, S. A., Highly dispersed pseudo-homogeneous and heterogeneous catalysts synthesized via inverse micelle solutions for the liquefaction of coal. SAND98-2630, p. 1–121, Sandia National Laboratories, Albuquerque, NM (1998).

Martino, A., Sault, A. G., Kawola, J. S., Boespflug, E., and Phillips, M. L., A sintering study of novel sol-gel nanocluster catalysts. *J. Catal.* **187,** 30 (1999).

Martino, A., Stoker, M., Hicks, M., and Bartholomew, C. H., Synthesis and characterization of Fe colloid catalysts in inverse micelle solutions. *Preprnt. Petrol. Div., Amer. Chem. Soc.* **40**(1), 78 (1995).

Martino, A., Yamanaka, S. A., Kawola, J. S., and Loy, D. A., Encapsulation of gold nanoclusters in silica materials via an inverse micelle/sol-gel synthesis. *Chem. Mater.* **9,** 423 (1997).

Masson, A., Bellamy, B., Romdhane, Y. H., Che, M., Roulet, H., and Dufour, G., Intrinsic size effect of platinum particles supported on plasma-grown amorphous alumina in the hydrogenation of ethylene. *Surf. Sci.* **173,** 479 (1986).

Matijevic, E., Control of powder morphology, *in* "Chemical Processing of Advanced Materials" (L. H. Hench and J. K. West, Eds.), p. 513. Wiley, New York (1992).

McNamara, W. B., Didenko, Y., and Suslick, K. S., Sonoluminescence temperatures during multibubble cavitation. *Nature* **401,** 772 (1999).

Mdleleni, M. M., Hyeon, T., and Suslick, K. S., Sonochemical synthesis of nanostructured molybdenum sulfide, *J. Am. Chem. Soc.* **120,** 6189 (1998).

Michalakos, P. M., Bellis, H. E., Brusky, P., Kung, H. H., Li, H. Q., Moser, W. R., Partenheimer, W., and Satek, L. C., Synthesis of vanadium phosphorus oxide catalysts by aerosol processing. *Ind. Eng. Chem. Res.* **34**(6) (1995).

Montejano-Carrizales, and Moran-Lopez, J. L., Geometrical characteristics of compact nanoclusters. *Nanostructured Mater.* **1,** 397 (1992).

Moser, W. R., Hydrodesulfurization Catalyst and Process Utilizing the Same, U.S. Patent 4,018,672, Assigned to Exxon (April 19, 1977).

Moser, W. R., Hydrodesulfurization Catalyst, U.S. Patent 4,090,982, Assigned to Exxon (May 23, 1978a).

Moser, W. R., Hydrodesulfurization of Oil Utilizing a Catalyst of Rare Earth Metal, Non-Rare Earth Metal and Alumina Support, U.S. Patent 4,092,239, Assigned to Exxon (May 30, 1978b).

Moser, W. R., Rare Earth Metal Oxide Hydrodesulfurization Catalysts, U.S. Patent 4,108,589, Assigned to Exxon (August 8, 1978c).

Moser, W. R., Reactor for High-Temperature Aerosol Decomposition and Catalysts and Other Materials Obtained, PCT Int. Appl., Assigned to Worcester Polytechnic Institute (1991).

Moser, W. R., Hydrocarbon partial oxidation catalysts prepared by the high-temperature aerosol decomposition process, *in* "Catalytic Selective Oxidation, ACS Symp. Ser." (S. T. Oyama and J. W. Hightower, Eds.), pp. 523, 244 (1993).

Moser, W. R., Preparation of Nanophase Solid State Materials, U.S. Patent 5,417,956, Assigned to Worcester Polytechnic Institute (May, 23, 1995a).

Moser, W. R., Process for the Preparation of Solid State Materials, U.S. Patent 5,466,646, Assigned to Worcester Polytechnic Institute (November 14, 1995b).

Moser, W. R., Developments in heterogeneous selective oxidation catalysis, *in* "New Developments in Selective Oxidation Catalysis," vol. 13, The Catalyst Group, Multi-client Study, Spring House, PA (1996).

Moser, W. R., and Cnossen, J. E., Aerosol propylene oxidation catalysts, *Preprnt. Pet. Chem. Div., Amer. Chem. Soc.* **37,** 1105 (1992).

Moser, W. R., and Connolly, K. E., Synthesis and characterization of copper modified zinc chromites by the high-temperature decomposition (HTAD) process for higher alcohol synthesis, *Chem. Eng. J.* **64,** 239 (1996).

Moser, W. R., Giang, T., Nguyen, S., and Kozyuk, O. V., A new route to cavitational chemistry and chemical processing by controlled flow cavitation, *in* "Process Intensification for the Chemical Industry, 3rd International Conference" (A. Green, Ed.), pp. 38, 173, BHR Group, London (1999).

Moser, W. R., Knapton, J. A., Koslowski, C. C., Rozak, J. R., and Vezis, R. H., Noble metal aerosol catalysts. *Preprnt. Pet. Chem. Div., Amer. Chem. Soc.* **38**(1), 829 (1993).

Moser, W. R., Knapton, J. A., Koslowski, C. C., Rozak, J. R., and Vezis, R. H., Noble metal catalysts prepared by the high-temperature aerosol decomposition (HTAD) process, *Catal. Today* **21,** 157 (1994).

Moser, W. R., and Lennhoff, J. D., Synthesis of mixed metal oxides for ceramics and catalysts by the HTAD process, *Proc. Mater. Res. Soc.,* Boston, MA (1984).

Moser, W. R., and Lennhoff, J. D., Synthesis of mixed metal oxides for ceramics and catalysts by the HTAD process. *Chem. Eng. Commun.* **83,** 241 (1989).

Moser, W. R., Lennhoff, J. D., Cnossen, J. E., Fraska, K., Schoonover, J. W., and Rozak, J. R., The preparation of advanced catalytic materials by aerosol processing, *in* "Advanced Catalysts and Nanostructured Materials, Novel Preparative Techniques" (W. R. Moser, Ed.), p. 535, Academic Press, New York (1996).

Moser, W. R., Lennhoff, J. D., Cnossen, J. E., Fraska, K., and Rozak, J. R., The high-temperature aerosol decomposition process: A general method for the synthesis of complex catalysts. *Preprnt. Petroleum. Div., Amer. Chem. Soc.* **40**(1), 49 (1995).

Moser, W. R., Marshik, B. J., Kingsley, J., Lemberger, M., Willette, R., Chan, A., Sundstrom IV, J. E., and Boye, A., The synthesis and characterization of solid-state materials produced by high shear hydrodynamic cavitation. *J. Mater. Res.* **10,** 2322 (1995).

Moser, W. R., Morikis, T., Zawadski, J., Sunstrom IV, J. E., and Marshik-Guerts, B. J., The synthesis of nanostructured, pure phase materials by hydrodynamic cavitation, *Third International Conference on Nanostructured Materials,* Kona, HI, 285 (1996).

Nikolajenko, V., Bosacek, V., and Danes, V., Investigation of properties of the metallic nickel surface in mixed Ni-MgO catalysts. *J. Catal.* **2,** 127 (1963).

Okuhara, T., Inumaru, K., and Misono, M., Active crystal face of vanadyl pyrophosphate for selective oxidation of *n*-butane, *in* "Catalytic Selective Oxidation" (S. T. Oyama and J. W. Hightower, Eds.), Vol. 523, p. 156, *Am. Chem. Soc. Symp. Ser.* (1993).

Salama, T. M., Hattori, H., Kita, H., Ebitani, K., and Tanaka, T., X-ray adsorption spectroscopic and electron paramagnetic resonance studies on the strong metal-support interaction of platinum supported on titania dispersed on silica, *J. Chem. Soc. Faraday Trans.* **89**(12), 2067 (1993).

Sanchez, R. M. T., Ueda, A., Tanaka, K., and Haruta, M., Selective oxidation of CO in hydrogen on gold supported on manganese oxide, *J. Catal.* **168,** 125 (1997).

Sault, A. G., Martino, A., Kawola, J. S., and Boesplug, E., Novel sol-gel based Pt nanocluster catalysts for propane dehydrogenation, *J. Catal.* **191,** 474 (2000).

Schultz, M., and Matijevic, E., Preparation and properties of nanosized PdS dispersions for electrolytic plating, *Colloids Surf.* **131,** 173 (1998).

Sellinger, A., Weiss, P. M., Nguyen, A., Lu, Y., Assink, R. A., Gong, W., and Brinker, C. J., Continuous, self-assembly of organic–inorganic nanocomposite coatings that mimic nature. *Nature* **394,** 256 (1998).

Siegel, R. W., Cluster assembled nanophase materials. *Annu. Rev. Mater. Sci.* **21,** 559 (1991).

Siegel, R. W., Nanophase materials, *in* "Encyclopedia of Applied Physics" (G. L. Trigg, Ed.), Vol. 11, p. 173, VCH Publishers, Weinheim (1994).

Siegel, R. W., and Hahn, H., Nanophase materials, *in* "Current Trends in the Physics of Materials" (M. Yussouff, Ed.), p. 403, World Scientific, Singapore (1987).

Skandan, G., Kear, B. H., Chang, W., and Hahn, H., Apparatus for making nanostructured ceramic powders and whiskers., U.S. Patent 5,514,350, Assigned to Rutgers University (May 7, 1996).

Sunstrom IV, J. E., Moser, W. R., and Marshik-Geurts, B. J., General route to nanocrystalline oxides by hydrodynamic cavitation, *Chem. Mater.* **8,** 2061 (1996).

Suslick, K. S., The mechanochemical effects of ultrasound, *Proc. Int. Conf. Mechanochem., 1st,* **1,** 43 (1993).

Suslick, K. S., Didenko, Y., Fang, M. M., Hyeon, T., Kolbeck, K. J., McNamara, W. B., Mdleleni, M., and Wong, M., Acoustic cavitation and its chemical consequences, *Phil. Trans. Royal Soc. A* **357,** 335 (1999).

Suslick, K. S., Fang, M., Hyeon, T., and Cichowlas, A. A., Nanostructured Fe-Co catalysts generated by ultrasound, *Mat. Res. Soc. Symp. Proc.* **351,** 443 (1994).

Suslick, K. S., Fang, M. M., Hyeon, T., and Mdleleni, M. M., Applications of sonochemistry to materials synthesis, *in* "Sonochemistry and Sonoluminescence" (L. A. Crum, T. J. Mason, J. Reisse, and K. S. Suslick, Eds.), p. 291, Kluwer Publishers, Dordrecht, Netherlands (1999).

Suslick, K. S., Hyeon, T., Fang, M., and Cichowlas, A., Sonochemical preparation of nanostructured catalysts, *in* "Advanced Catalysts and Nanostructured Materials: Modern Synthetic Methods" (W. R. Moser, Ed.), p. 197, Academic Press, San Diego. (1996).

Sze, C., Gulari, E., and Demczyk, B. G., Surface structure–catalytic function in nanophase gold catalysts, *in* "Nanophase and Nanocomposite Materials" (S. Komarneni, J. C. Parker, and G. J. Thomas, Eds.), Vol. 286, p. 143, *Mater. Res. Soc.* (1993).

Tompa, G. S., Skandan, G., Glumac, N., and Kear, B. H., A new flame process for producing nanopowders, *Amer. Ceram. Soc. Bull.* (October) 70 (1999).

Tschöpe, A., Schaadt, D., Birringer, R., and Ying, J. Y., Catalytic properties of nanostructured metal oxides synthesized by inert gas condensation, *Nanostr. Mater.* **9,** 423 (1997).

Tschöpe, A., Ying, J. Y., and Tuller, H. L., *Symposium B on Materials for Sensors: Functional Nanoscaled Structures,* Saarbruecken, Germany, 111 (1996).

Tsubota, S., Cunningham, D. A. H., Bando, Y., and Haruta, M., Preparation of nanometer gold strongly interacted with titania and the structure sensitivity in low-temperature oxidation of CO, *in* "Studies in Surface Science and Catalysis, Preparation of Catalysts VI" (G. Poncelet, J. Martens, B. Delmon, P. A. Jacobs, and P. Grange, Eds.), Vol. 91, p. 227, Elsevier, Amsterdam (1995).

Tsubota, S., Ueda, A., Sakurai, H., Kobayashi, T., and Haruta, M., Applications of supported gold catalysts in environmental problems, *in* "Environmental Catalysis" (J. N. Armor, Ed.), Vol. 552, p. 420, Amer. Chem. Soc., Symp. Ser. (1994).

Van Hardeveld, R., and, F. Hartog, Influence of metal particle size in nickel-on-aerosil catalysts on surface site distribution, catalytic activity, and selectivity, *Adv. Catal.* **22,** 75 (1972).

van Santen, R. A., and Niemantsverdriet, J. W., "Chemical Kinetics and Catalysis," Plenum press, New York (1995).

Volta, J. C., Desquesnes, W., Moraweck, B., and Coudurier, G., A new method to obtain supported oriented oxides: MoO_3 graphite catalysts in propylene oxidation to acrolein, *React. Kinet. Catal. Lett.* **12,** 241 (1979).

Volta, J. C., and Tatibouet, J. M., Structure sensitivity of MoO_3 in mild oxidation of propylene, *J. Catal.* **93,** 467 (1985).

Wang, C.-C., and Ying, J. Y., Sol-gel synthesis and hydrothermal processing of anatase and rutile titania nanocrystals, *Chem. Mater.* **11,** 3113 (1999).

Wilcoxon, J. P., Martino, A., Baughman, R. L., Klavetter, E., and Sylwester, A. P., Synthesis of transition metal clusters and their catalytic and optical properties, *in* "Nanophase and Nanocomposite Materials" (S. Komarneni, J. C. Parker, and G. J. Thomas, Eds.), Vol. 286, p. 131, Mater, Res. Soc. Symp. Proc. (1993).

Wilcoxon, J. P., Williamson, R. L., and Baughman, R. J., Optical properties of gold colloids formed in inverse micelles. *J. Chem. Phys.* **98,** 9933 (1993).

Williamson, G. K., and Hall, W. H., Crystallographic strain determination by X-ray diffraction, *Acta Metall.* **1,** 22 (1953).

Wold, A., Gao, Y.-M., Miller, D., Kershaw, R., and Dwight, K., Synthesis of catalytic materials by spray pyrolysis, *in* "Advanced Catalysts and Nanostructured Materials: Novel Preparative Techniques" (W. R. Moser, Ed.), p. 505, Academic Press, San Diego (1996).

Woodward, R. B., and Hoffmann, R., "The Conservation of Orbital Symmetry," Academic Press, New York (1970).

Ying, J. Y., and Tschöpe, A., Gas phase synthesis of nonstoichiometric nanocrystalline catalysts, *in* "Advanced Catalysts and Nanostructured Materials: Modern Synthetic Methods" (W. R. Moser, Ed.), p. 231, Academic Press, San Diego (1996).

Young, F. R., "Cavitation," McGraw-Hill, New York (1989).

Zarur, A. J., Hwu, H. H., and Ying, J. Y., Reverse microemulsion-mediated synthesis and structure evolution of barium hexaaluminate nanoparticles, *Langmuir* **16,** 3042 (2000).

Zarur, A. J., and Ying, J. Y., Reverse microemulsion synthesis of nanostructured complex oxides for catalytic combustion, *Nature* **403,** 65 (2000).

Zhang, Z., Wang, C.-C., Zakaria, R., and Ying, J. Y., Role of particle size in nanocrystalline TiO_2-based photocatalysts, *J. Phys. Chem. B* **102**(52), 10871 (1998).

Zhao, M., and Crooks, R. M., Dendrimer-encapsulated Pt nanoparticles, synthesis characterization, and applications to catalysis, *Adv. Mater.* **11,** 217 (1999a).

Zhao, M., and Crooks, R. M., Homogeneous hydrogenation catalysis using monodisperse, dendrimer-encapsulated Pd and Pt nanoparticles, *Angew. Chem. Int. Ed.* **38,** 364 (1999b).